Response to reviewer 1

We would like to thank the reviewer for the time and effort spent reading our manuscript and for the useful comments and suggestions. A detailed response to all comments can be found below, where the black text indicates comments of the reviewer. The blue text denotes our response to these comments; line numbers refer to the revised version of the paper.

Comments by the reviewer:
General Comments: Excellent work, taking into account that the diapygnal fluxes at the interfaces of the stepped structures are considered comparable to those of the surface fluxes. The further use of the current results (in a next paper) can provide at global scale the contribution of the stepped structure diapygnal fluxes.

We indeed are working on a next paper where we compute the contribution of double-diffusive processes to the global mechanical energy budget. Furthermore, we noticed that 'interfaces' is a more widely accepted term than gradient layers. Therefore, we replaced all mentions of 'gradient layers' by 'interfaces' throughout the manuscript. This included replacements in Figure 4, 5, 6, and 8.

Specific Comments: A sentence is needed why only Argo floats and ice tethered profilers were used. Why not the high vertical resolution of the CTD profiles, which in most cases the vertical profiles are deeper than those of the floats.

We limited ourselves to Argo floats and Ice-Tethered Profilers, because they have a global coverage and we could use them to show that the algorithm performs its task well. However, we agree with the reviewer that it would be interesting to extend the dataset with more data in the future. We also added a sentence to the conclusions to highlight this possibility.

> *Lines 266-268:*
> *'Therefore, when considering an individual staircase region, we recommend optimizing the input variables of the algorithm for that specific region and applying the algorithm on additional data, for example high-resolution CTD or microstructure profiles, where available.'*

Furthermore, we added additional information about the original vertical resolution of the profiles used in this study (Fig. 1 and Table 1). We added the Figure and Table at the end of this response.

> *Lines 54-58:*
> *'Details on the origin and vertical resolution of the profiles are depicted in Table 1 and Figure 1, in which Figure 1b confirms that all profiles have observations deeper than 500 dbar. Furthermore, the average vertical resolution of the profiles indicates the average resolution is well below the 5 dbar that was used as a threshold (Fig. 1c). After this quality control, 487,493 vertical temperature and salinity profiles remain.'*

Before or after the Figure 6, add a sentence about the depth the stepped structures were detected, i.e. diffusive convection mostly was detected at depths between 300-400 m, while the salt finger between 400-700 m.

We rewrote the paragraph to clarify that we selected the staircases with most steps. In addition, we indicated the water masses between which these staircases are found (and provided references):

> *Lines 164-167:*
> *'In line with previous results (Rudels, 2015), staircases in the diffusive-convective regime (Fig. 7a) are mainly detected on the thermocline with the conservative temperature increasing with depth. These staircases are predominantly located in the Arctic Ocean at a depth between 300-400 m, which is between the warm and saline Atlantic Water and cold and fresh surface waters (Rudels, 2015)'*
>
> *Lines 175-178:*
> *'Thermohaline staircases with a high number of steps in the salt-finger regime are detected on the main thermocline where the conservative temperature decreases with depth (Fig. 7b). Compared to the staircases in the diffusive-convective regime, these staircases are located slightly deeper at 400-700 m. While the locations of these staircases vary, they are located above the cold and fresh Antarctic Intermediate Water, which is observed below 700 m (Tsuchiya, 1989; Fine, 1993; Talley, 1996).*

Will be of interesting to see in a new paper using the CTD data from the SeaDataNetand or EMODNET portals applying the same technology of this ms to reveal the deepest stepped structures, as well as the fluxes estimates.

We agree with the reviewer that it would be interesting to use the algorithm on different datasets as well, but this is outside the scope of the present paper. No changes in text.

Table 1 Number of floats and profiles in the global dataset. Profiles taken with Argo floats are categorised by the Data Assembly Center (DAC). Profiles taken with Ice-Tethered Profilers are categorised as ITP. The percentage between brackets indicates the relative contribution to the total number of profiles in the global dataset (487,493 profiles). More details on abbreviations of DAC can be found in Argo (2019)

DAC	Number of floats	profiles
aoml	2692	312,285 (64.1%)
bodc	93	11,092 (2.3%)
coriolis	347	27,134 (5.6%)
csio	81	15,099 (3.1%)
csiro	378	42,942 (8.8%)
incois	65	4,363 (0.9%)
jma	205	22,919 (4.7%)
kma	1	1 (0.0%)
kordi	0	0 (0.0%)
meds	145	9,285 (1.9%)
nmdis	0	0 (0.0%)
ITP	82	42,373 (8.7%)

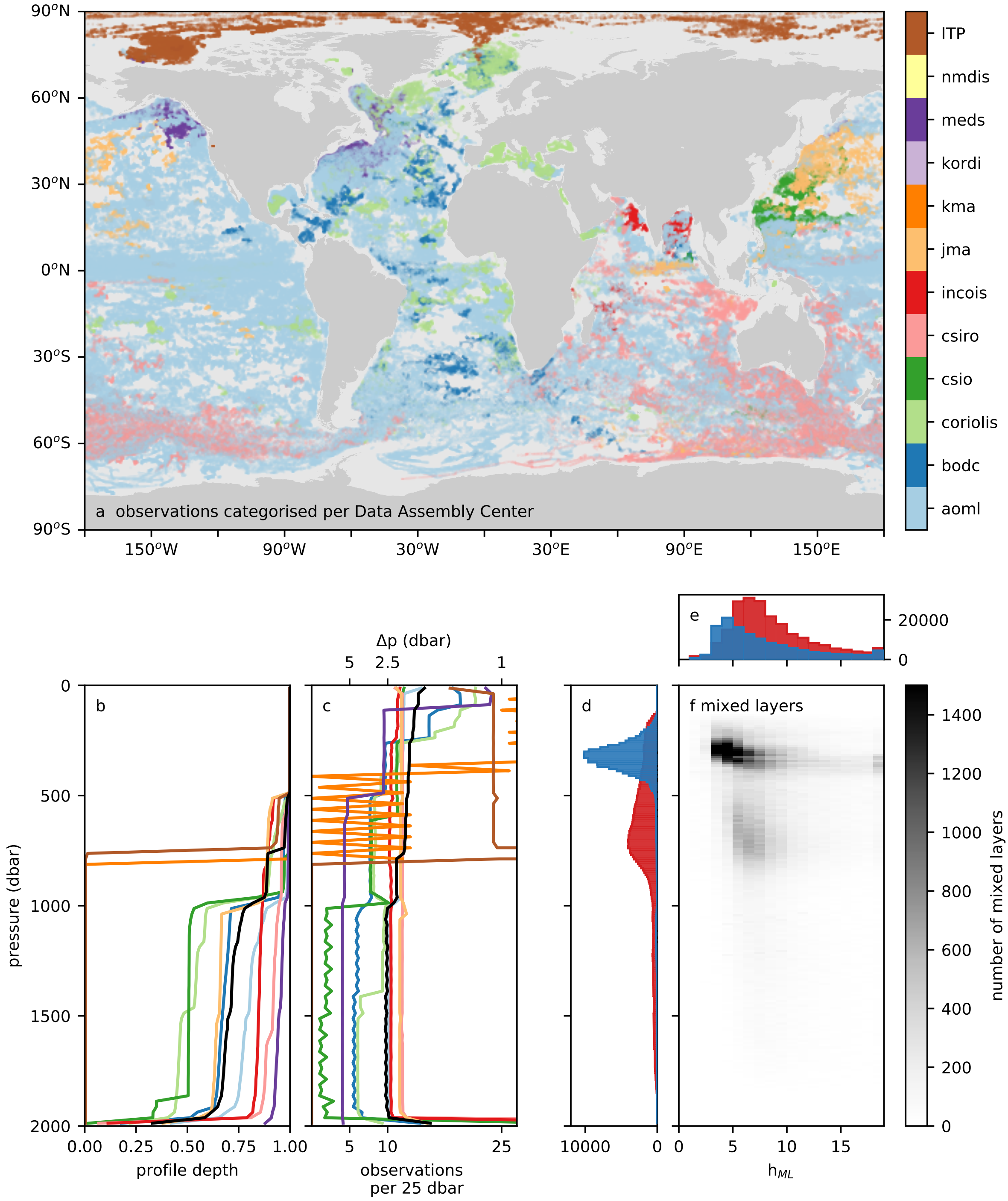

Figure 1 (a) Locations of observations categorised by Data Assembly Centers (DAC) when obtained by an Argo float. Profiles obtained with Ice-Tethered Profilers are indicated with ITP. (b) Cumulative fraction of profiles that reached a given pressure in 25-dbar intervals from 0 to 2,000 dbar per DAC. (c) Average number of observations in 25-dbar intervals from 0 to 2,000 dbar. (d) Distribution of detected mixed layer pressures in the salt-finger (red histogram) or diffusive-convective (blue histogram) regime. (e) Number of detected mixed layers height in the salt-finger (red histogram) or diffusive-convective (blue histogram) regime. (f) Distribution of detected mixed layer heights in thermohaline staircases per pressure level. Panels (b) and (c) were obtained following Wong et al. (2020). Black lines indicate the averages in total global dataset. More details on abbreviations of DAC can be found in Argo (2019)

Response to reviewer 2

We would like to thank the reviewer for the time and effort spent reading our manuscript, and for the comments which have improved the manuscript significantly. A detailed response to all comments can be found below, where the blue text indicates our response to the reviewers' comments, which are denoted in black. Line numbers correspond to the revised manuscript.

Comments by the reviewer:

This paper tackles the worthwhile problem of identifying and characterizing double-diffusive staircase structures in ocean temperature and salinity profiles. Unfortunately there are fundamental shortcomings of the work.

Without seeing representative profiles (from different regions), it is impossible to determine the extent to which the algorithm works. Figure 6b provides clues that it maybe appropriate sometimes for the identification of salt-finger layers, although there are profile regions that appear to indicate steps which are not colored red (and it is unclear why). It would be helpful to be given some information about where the profiles are, and shown the detailed T-S structure.

The algorithm does detect thermohaline staircases not only using profiles of conservative temperature, but also using potential density and absolute salinity. Therefore, it is not always clear from conservative temperature profiles why a step is disregarded. To be more transparent about this selection, we added 3 figures in the Appendix of the revised paper with representative profiles of three well-known formation regions: the Arctic Ocean, the Mediterranean Sea, and the western tropical Atlantic Ocean. In these figures, we show the different steps of the algorithm. We also added the figures at the end of this reply.

Figure 6a is clearly showing that the algorithm is not working. The algorithm appears to have picked up the thermohaline intrusions underlying the double-diffusive staircase. One can see this immediately because of the regions that are deeper than the temperature maximum are marked blue. I would encourage the reviewers to examine some papers on the Arctic staircase and compare and validate their results against those. Similarly, the reader needs to see detailed profiles and validation.

Apparently, the algorithm was not clearly explained in the original paper and we use this comment to better explain the working and results of the algorithm (below and in the revised paper).

The algorithm detects stepped structures from vertical profiles of conservative temperature and absolute salinity. This implies that the algorithm can also detect mixed layers arising from thermohaline intrusions. Therefore, we added a paragraph to the introduction to discuss the origin of thermohaline staircases:

> *Lines 17-23:*
> *'It is still a topic of discussion how double-diffusive convection leads to the formation of thermohaline staircases in oceanic environments (Merryfield, 2000). For example, Stern (1969) argued that small-scale mixing processes trigger the formation of internal waves. On the other hand, variations in the turbulent heat and salt fluxes (Radko, 2003) or in the counter-gradient buoyancy fluxes that sharpen density*

gradients (Schmitt, 1994) could also lead to the formation of thermohaline staircases. Lastly, subsurface mixed layers can also arise from thermohaline intrusions (Merryfield, 2000). Although it remains unclear how these staircases arise, these studies agree that the formation of these subsurface mixed layers are related to double-diffusive processes.'

We also added a sentence to highlight the benefit of using a detection algorithm based on the vertical structure, such that the Turner angle can be used for validation:

Lines 74-75:
'The benefit of using the vertical structure, instead of using assumptions based on the Turner angle, is that we can use this angle to verify the results.'

We want to emphasize that our results show that most detected staircases are within double-diffusive regimes (Fig. 6). This suggests that we predominantly detect double-diffusive thermohaline staircases. However, similar to any other detection of thermohaline staircases, we cannot determine whether the origin of a subsurface mixed layer in double-diffusive regimes arises from thermohaline intrusions or from double-diffusive mixing. We added a paragraph to Section 3 and rephrased two sentences in the abstract and introduction to clarify this.

Line 1:
'Thermohaline staircases are associated with double-diffusive mixing.'

Lines 12-14:
'They are associated with double-diffusive processes, which in turn result from a two orders of magnitude difference between the molecular diffusivity of heat and that of salt (Stern, 1960).'

Line 167-174:
'Figure 7a also indicates that the deepest mixed layer of some thermohaline staircases is located at the temperature maximum, which suggests that this lowest layer might be the result of thermohaline intrusions (Ruddick and Kerr, 2003). There, the algorithm identified a mixed layer, because temperature and salinity stratification were weak enough (see Section 3.1). Furthermore, both conservative temperature and absolute salinity in this mixed layer are larger than in the mixed layer above. While both are typical for a staircase in the diffusive-convective regime, the algorithm does not detect whether this mixed layer is a temperature maximum, which could indicate that arose from thermohaline intrusions. Note that this only concerns the deepest mixed layers of the staircases, and that only the characteristics of the interfaces in between mixed layers are labelled as part of a staircase by the algorithm.'

Furthermore, we would like to note that it is difficult to design a staircase detection algorithm that is optimized for all staircase regions, due to large variations in the height of the mixed layers and temperature and salinity steps of the interfaces. In this global dataset, we aimed to optimize the global detection, such that we detect thermohaline staircases in all well-known formation regions. To show this in a transparent way, we added figures of representative profiles (Figure A1, A2, A3), and added a paragraph to the conclusions to discuss this issue.

Lines 260-268:

‘We optimized the input of the algorithm such that it provides a global overview and limits the number of detected false positives. As a result, the regional verification in Section 5 indicated that the data pre-processing and data analysis have some limitations. For example, the vertical resolution of 1 dbar in the profiles is too course to capture all staircase steps in the Arctic Ocean. In the Mediterranean, the Argo floats did not dive deep enough to capture the full depth of the staircase region. However, the fact that (i) the algorithm detects thermohaline staircases at realistic depth ranges, with (ii) conservative temperature and absolute salinity steps across the interfaces, and in (iii) the same double-diffusive regime as previous studies (Table 3-Table 5), indicates that the algorithm itself performs well. Therefore, when considering an individual staircase region, we recommend optimizing the input variables of the algorithm for that specific region and applying the algorithm on additional data, for example high-resolution CTD or microstructure profiles, where available.’

(As an aside, potential temperature should be used when ex-amining step structures in deep water and the authors ought to compare profiles of potential temperature and temperature through deep staircases.)

It is not entirely clear to us why the reviewer insists that potential temperature should be used when examining step structures in deep water. We prefer to use conservative temperature over potential temperature, because thermohaline staircases are predominantly studied for their heat and salt fluxes through the interfaces. In contrast to potential temperature, conservative temperature can be regarded as a conservative variable and can be accurately used for computations regarding the heat content (Graham and McDougall, 2013). For further details on the conservative temperature, we refer to Graham and McDougall (2013):

Graham, F. S., & McDougall, T. J. (2013). Quantifying the nonconservative production of Conservative Temperature, potential temperature, and entropy. Journal of Physical Oceanography, 43(5), 838-862. https://doi.org/10.1175/JPO-D-11-0188.1

To clarify that we use conservative temperature instead of potential temperature, we replaced ‘temperature’ by ‘conservative temperature’ and ‘salinity’ by ‘absolute salinity’ throughout the manuscript.

Furthermore, we added a sentence to motivate the usage of conservative temperature:

Line 63-64:
‘Note that we use conservative temperature as this is more accurate than potential temperature in computations concerning heat fluxes and heat content (Graham and McDougall, 2013).’

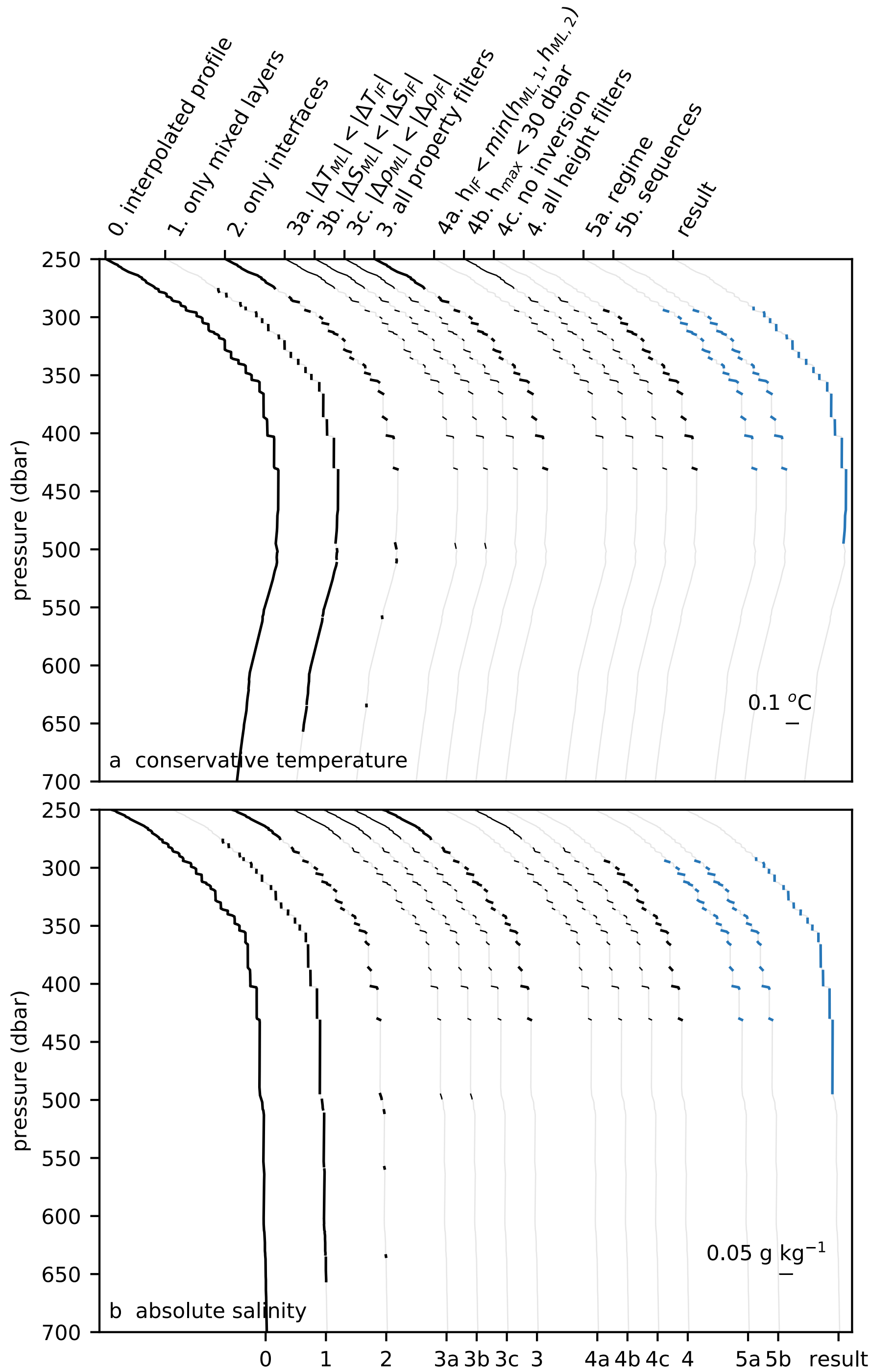

Figure A 1 Steps of the detection algorithm applied on a profile in the Arctic Ocean, where steps are indicated on separate (a) conservative temperature and (b) absolute salinity profiles. Each profile is shifted for clarity. Similar to Figures 3-5, an interface is not considered by the detection algorithm when the interface characteristics did not meet the requirements of a previous step. Original profile is taken from Ice-Tethered-Profiler ITP64 at 137.8°W and 75.2°N on 29 January 2013. The details of the pre-processing and the algorithm steps are discussed in Section 2 and Section 3, respectively.

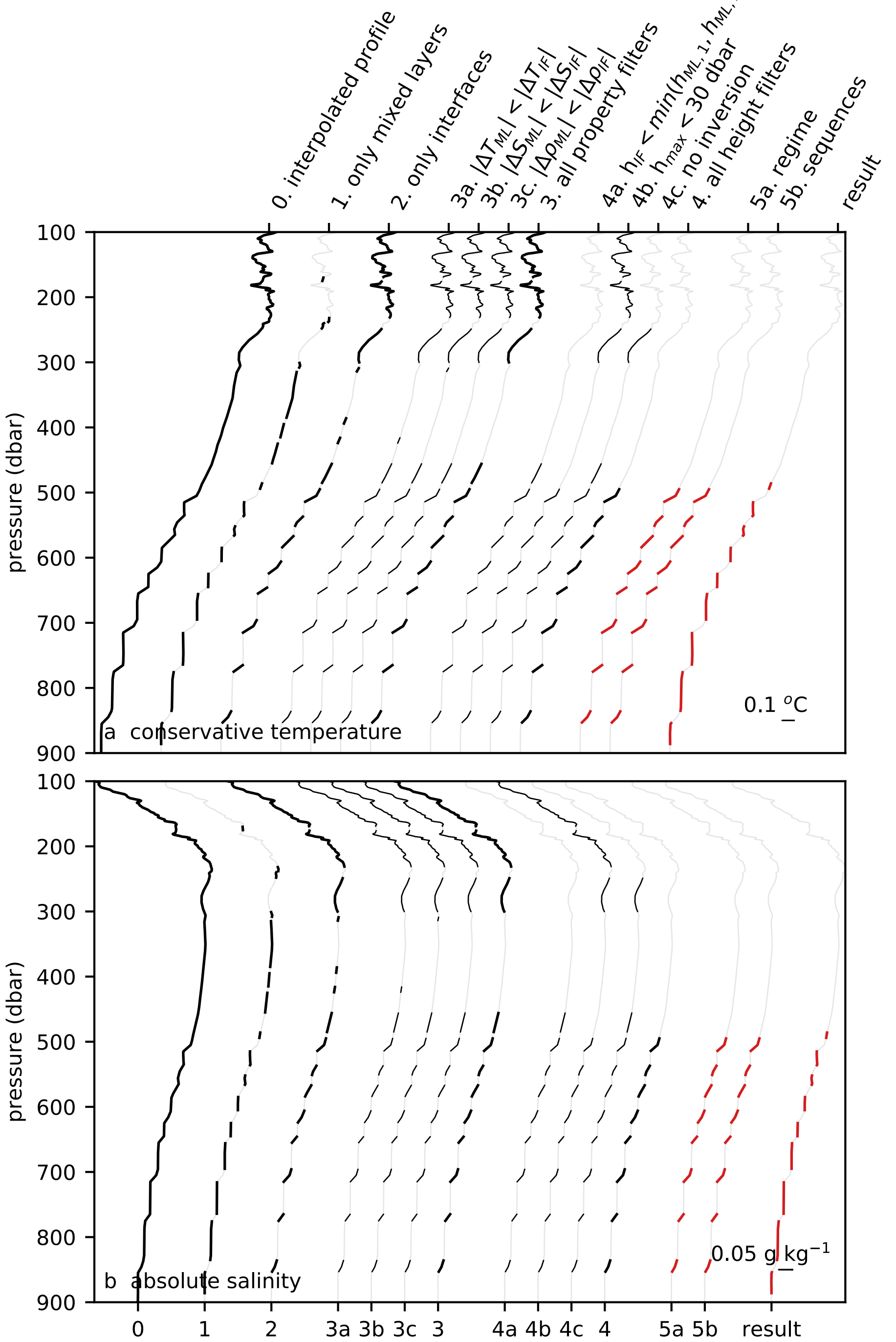

Figure A 2 as Figure A1, but for a profile in the Mediterranean Sea. Original profile is taken from Argo float 6901769 at 8.9^{o}E and 37.9^{o}N on 31 October 2017.

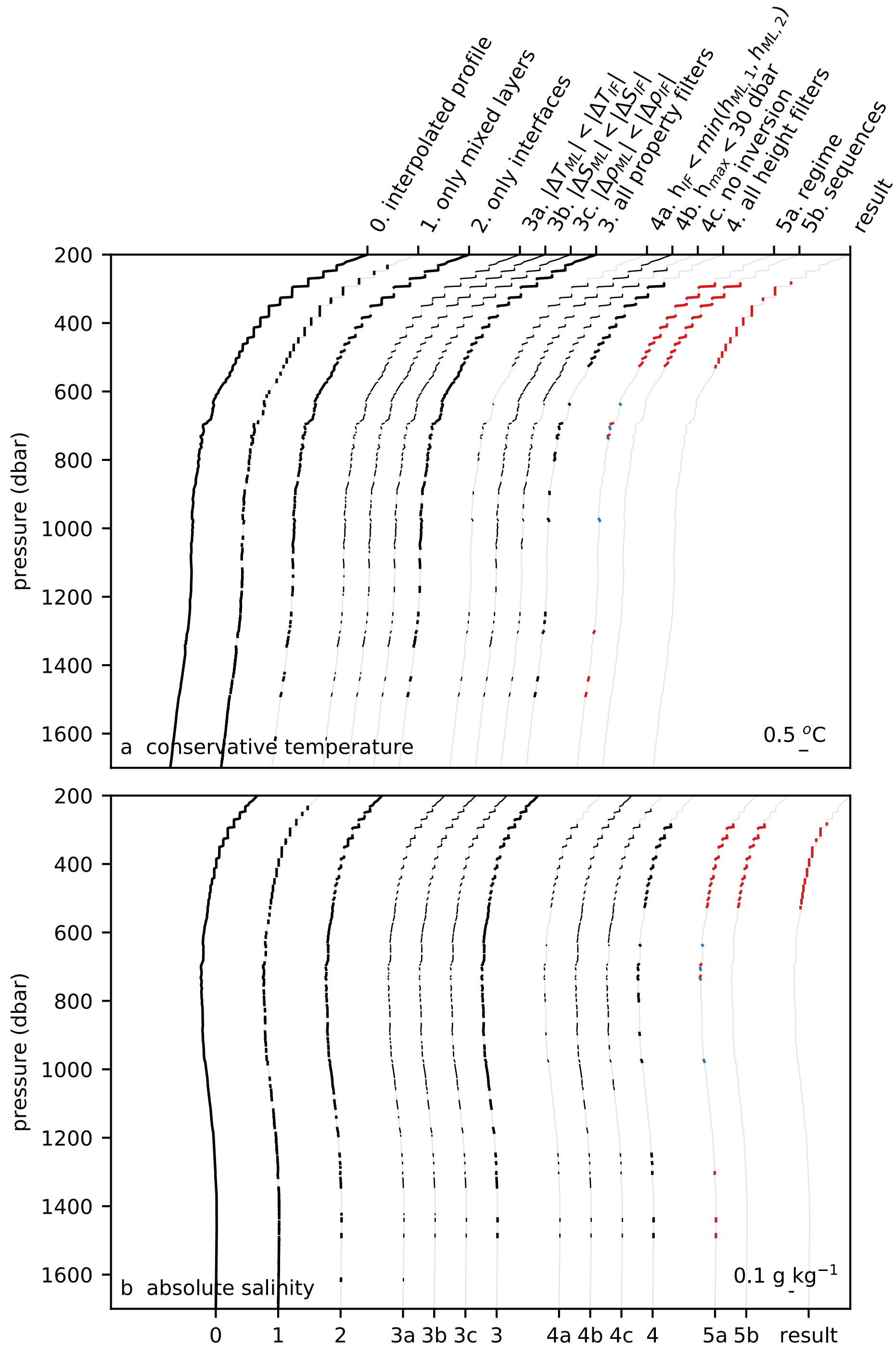

Figure A 3 as Figure A1, but for a profile in the western tropical North Atlantic. Original profile is taken from Argo float 4901478 at 53.3°W and 11.6°N on 9 August 2014.

Response to Reviewer 3

We would like to thank the reviewer for the time and effort spent reading our manuscript, and for the comments which have improved the manuscript significantly. A detailed response to all comments can be found below, where the blue text indicates our response to the reviewers' comments, which are denoted in black. Line numbers correspond to the revised manuscript.

Comments by the reviewer:

This paper describes the creation of a novel dataset to study thermohaline staircases inthe ocean. It is a great example of how something new can be brought out of a widely-used dataset through a suitable data processing technique. The data processing is careful and well documented, and compares favorably against earlier regional studies. In particular, Figure 5 is impressive, where the authors appear to capture the salt-fingering and double-diffusive convection regimes based on the application of theirstraightforward criteria. The dataset created by the authors is quite unique and willundoubtedly be of use to others, particularly since it is distributed together with thesoftware. I believe it should be published with minor revisions.

There are a few points I would like the authors to address.

– What is the estimated precision of the salinity, temperature, and density measurements, and how does this compare with typical step sizes? I ask because, if the precisions are coarse, or upstream rounding or truncation has been applied, a jump-like effect mimicking staircases could arise as an artifact. Here I think it is important to explicitly examine the measurement precisions and noise levels to rule out this possibility, rather than to simply argue that the final product seems to be physically meaningful.

The accuracy of a temperature measurement in an Argo float or Ice-Tethered Profiler is 0.001°C; for salinity this is 0.001 psu. These errors are much smaller than typical temperature and salinity differences characterizing staircases and hence roundoff due to measurement error does not play a role in step detection.

– As the software is an important part of this contribution, I think it should be described in more detail, with language, license, and function or function names listed, together with a description of how the software is to be used and possibly listing inputs and outputs. It is important that the software is arranged as a function or functions rather than as a script, if it is to be useful to others.

We thank the reviewer for this suggestion. We added a figure with the structure of the software and a table with the separate functions of the software (Table A2). The figure with the structure of the software is also added at the end of this reply. We have added the license and language at the code availability.

> *Lines 281-284:*
> *'Both algorithm and global dataset are available at doi: https://doi.org/10.5281/zenodo.4286170 (van der Boog et al., 2020). The algorithm is written in Python3 and is available under the Creative Commons Attribution 4.0 License. More details on the functions and output of the algorithm are depicted in Table A1 and Table A2, respectively. The structure of the algorithm is displayed in Figure A4. '*

–I find it conspicuous that, zooming on on Fig. 6a, I see a lot of staircases that appear to have been missed, lying just above the blue curves showing detections. Please discuss these and whether or not they are 'false negatives' that the method should detect but does not, and if they are then explain why such false negatives are acceptable.

We agree with the reviewer that it is not entirely clear from Figure 7a why some mixed layers are missed by the algorithm. A small part of these mixed layers is missed due to the resolution of the original profiles. We have clarified this in the text.

> *Lines 224-226:*
> *'Due to the vertical resolution of the profiles and the design of the algorithm (recall that the mixed layers are separated from each other by removing the upper and lower datapoint of the mixed layer, Section 3.1), the method is not capable of detecting very thin interfaces (Figure A1).'*

The other part of the mixed layers is missed because the algorithm detects thermohaline staircases not only using profiles of conservative temperature (as shown in Figure 7a), but also using potential density and absolute salinity. Therefore, it is not always clear from conservative temperature profiles why a step is disregarded. To be more transparent about this selection, we added 3 figures in the Appendix of the revised paper with representative profiles of three well-known formation regions: the Arctic Ocean, the Mediterranean Sea, and the western tropical Atlantic Ocean. In these figures, we show the different steps of the algorithm. We also added the figures at the end of this reply.

–The problem that the authors examine is a difficult one. I am not sure that the most elegant solution has been found, as it is dependent upon the choices of a number of free parameters. Ideally, one should not have to specify a prior cutoffs; it would be preferable for these to emerge from the data based on examining statistical distributions. However, a parameter-free version of this product would probably take a great deal of more work and possibly different methods (e.g., least squares fits, statistical tests, etc.), and it is much better to have a satisfactory solution than none at all.

Yes, we agree with the reviewer. The algorithm mainly depends on the parameters to detect the mixed layers (Fig. 8). It would indeed be more elegant to remove all parameters from the algorithm, but this is outside the scope of this paper.

Because the authors have thought a lot about this problem, they are in a good position to describe the shortfalls of the current method and how it might be improved in the future. This would be a great topic to discuss at the end of the paper.

The major shortfall of the algorithm is the preprocessing of the data and, consequently, the vertical resolution. We now discuss this shortfall, and how to resolve it, in the revised text.

> *Lines 260-268:*
> *'We optimized the input of the algorithm such that it provides a global overview and limits the number of detected false positives. As a result, the regional verification in Section 5 indicated that the data pre-processing and data analysis have some*

limitations. For example, the vertical resolution of 1 dbar in the profiles is too course to capture all staircase steps in the Arctic Ocean. In the Mediterranean, the Argo floats did not dive deep enough to capture the full depth of the staircase region. However, the fact that (i) the algorithm detects thermohaline staircases at realistic depth ranges, with (ii) conservative temperature and absolute salinity steps across the interfaces, 265 and in (iii) the same double-diffusive regime as previous studies (Table 3-Table 5), indicates that the algorithm itself performs well. Therefore, when considering an individual staircase region, we recommend optimizing the input variables of the algorithm for that specific region and applying the algorithm on additional data, for example high-resolution CTD or microstructure profiles, where available.'

Minor comments

p 1, first paragraph, and p 2 line 31, "double-diffusive" should be hyphenated

Corrected throughout the manuscript. Following the same grammar rule, we replaced Ice Tethered Profilers by Ice-Tethered Profilers.

p 1, line 14, "two orders of magnitude"

Corrected (line 13).

p 1, line 17, and p 5, line 93, "of the order"

Corrected (line 16, line 106).

p 1, line 19, "the the"

Corrected (line 24).

p 2, line 35, would recommend present tense

We agree, we changed the tense.

p 2, line 47, what is the gray list and where can it be found?

The gray list is a list of Argo floats that have problems with one or more sensors. We have mentioned this in the revised manuscript:

Lines 51-53:
'First a quality check is performed, where a profile is excluded from analysis if it was taken by an Argo float mentioned on the grey list. This grey list contains floats that may have problems with at least one of the sensors (https://www.nodc.noaa.gov/argo/grey_floats.htm).'

p 3, line 57, this is a second moving average, yes?

No, this is a first moving average, instead of the 200 dbar. We have clarified this in the text.

> *Lines 67-68:*
> *'The Turner angle is computed using profiles that were smoothed with a moving average of 50 dbar instead of 200 dbar'*

p 3, eqn 1, what is the meaning of the overbar?

The overbar indicated that the temperature and salinity profiles were smoothed. We understand that this is unclear, and the overbar is not necessary. Therefore, we decided to remove the overbar from equation 1.

p 4, lines 64, "the properties of any layer lying between" would be better

We thank the reviewer for this suggestion. We rephrased the sentence:

> Lines 78-79:
> *'Next, the properties of any layer lying between the mixed layers (the interfaces, IF, orange dots in Fig. 3) are assessed by applying a minimum in temperature and salinity variations.'*

p 4, lines 74,75, and 76, "criterium" should be "criterion"

Corrected (lines 86, 87, and 90).

p 7, I believe the first paragraph is unnecessarily repeated

Yes, we agree. We have changed the first paragraph and removed all repetitions.

> *Lines 129-133:*
> *'Furthermore, the tallest observed interfaces are found in the Mediterranean Sea with heights up to h_{IF} = 27 m, where they separate mixed layers of over 100 m (Zodiatis and Gasparini, 1996; Radko, 2013). To prevent false detection of large vertical interfaces of up to hundreds of meters, we limit the interface height to $h_{IF,max}$ = 27 dbar (Table 2, Fig. 5b). This only affects the classification of 1 % of the interfaces (Fig. 5b).'*

p 10, where are these example profiles from?

We have added a paragraph with more details on the profiles.

> *Lines 162-165:*
> *'In line with previous results (Rudels, 2015), staircases in the diffusive-convective regime (Fig. 7a) are mainly detected on the thermocline with the conservative temperature increasing with depth. These staircases are predominantly located in the*

Arctic Ocean at a depth between 300-400 m, which is between the warm and saline Atlantic Water and cold and fresh surface waters (Rudels, 2015).'

Lines 175-178:
'Thermohaline staircases with a high number of steps in the salt-finger regime are detected on the main thermocline where the conservative temperature decreases with depth (Fig. 7b). Compared to the staircases in the diffusive-convective regime, these staircases are located slightly deeper at 400-700 m. While the locations of these staircases vary, they are located above the cold and fresh Antarctic Intermediate Water, which is observed below 700 m (Tsuchiya, 1989; Fine, 1993; Talley, 1996).'

p 11 "optimalization" should be "optimization"

Corrected (line 213).

p 13, line 219–220, I am not sure what is being meant here. It seems a lot of physical assumptions have been made that are implicit in the parameter choices.

We meant that we, in contrast to previous detection algorithms, do not select on the Turner angle. We rephrased the sentence:

Lines 257-258:
'Note that by formulating the algorithm solely on this vertical structure of the staircases, we could use the Turner angle of the detected staircases for verification.'

p 14, line 225 should say "both double-diffusive regimes" I believe Table A1, Julian should be capitalized and density should not be

Corrected (line 270).

Many of the references have incorrectly capitalized titles or journal names.

Corrected.

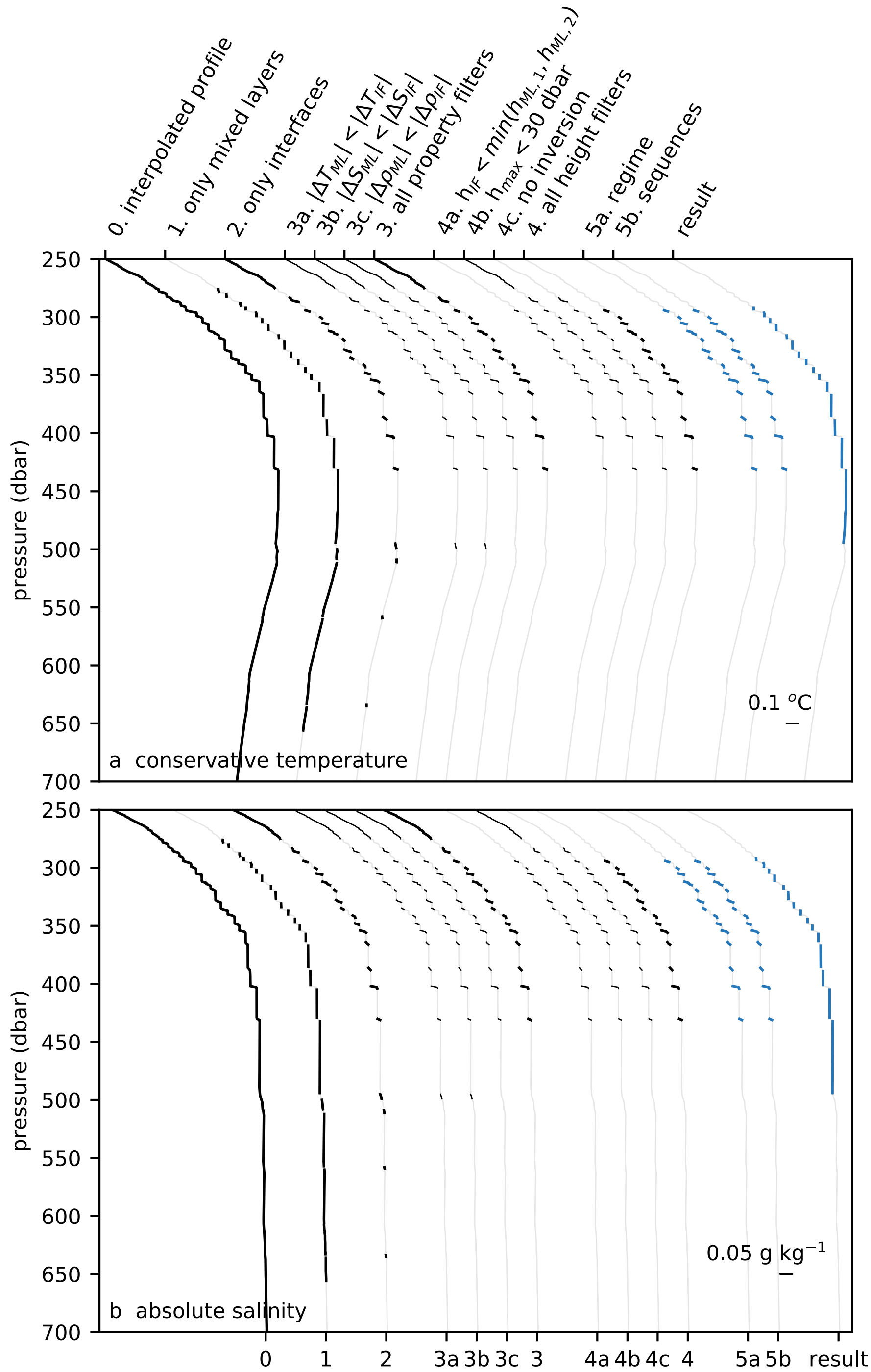

Figure A 4 Steps of the detection algorithm applied on a profile in the Arctic Ocean, where steps are indicated on separate (a) conservative temperature and (b) absolute salinity profiles. Each profile is shifted for clarity. Similar to Figures 3-5, an interface is not considered by the detection algorithm when the interface characteristics did not meet the requirements of a previous step. Original profile is taken from Ice-Tethered-Profiler ITP64 at 137.8°W and 75.2°N on 29 January 2013. The details of the pre-processing and the algorithm steps are discussed in Section 2 and Section 3, respectively.

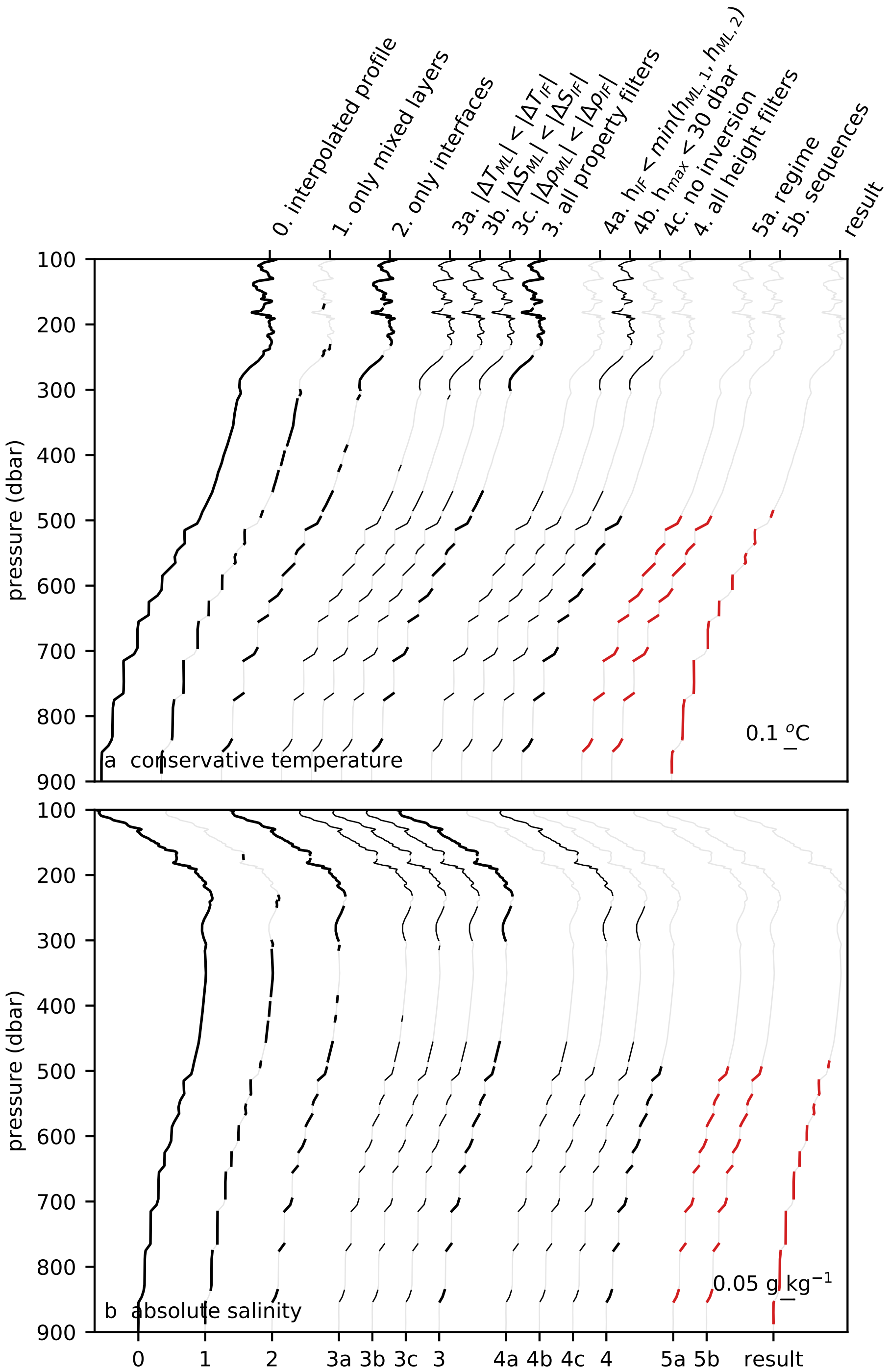

Figure A 5 as Figure A1, but for a profile in the Mediterranean Sea. Original profile is taken from Argo float 6901769 at 8.9°E and 37.9°N on 31 October 2017.

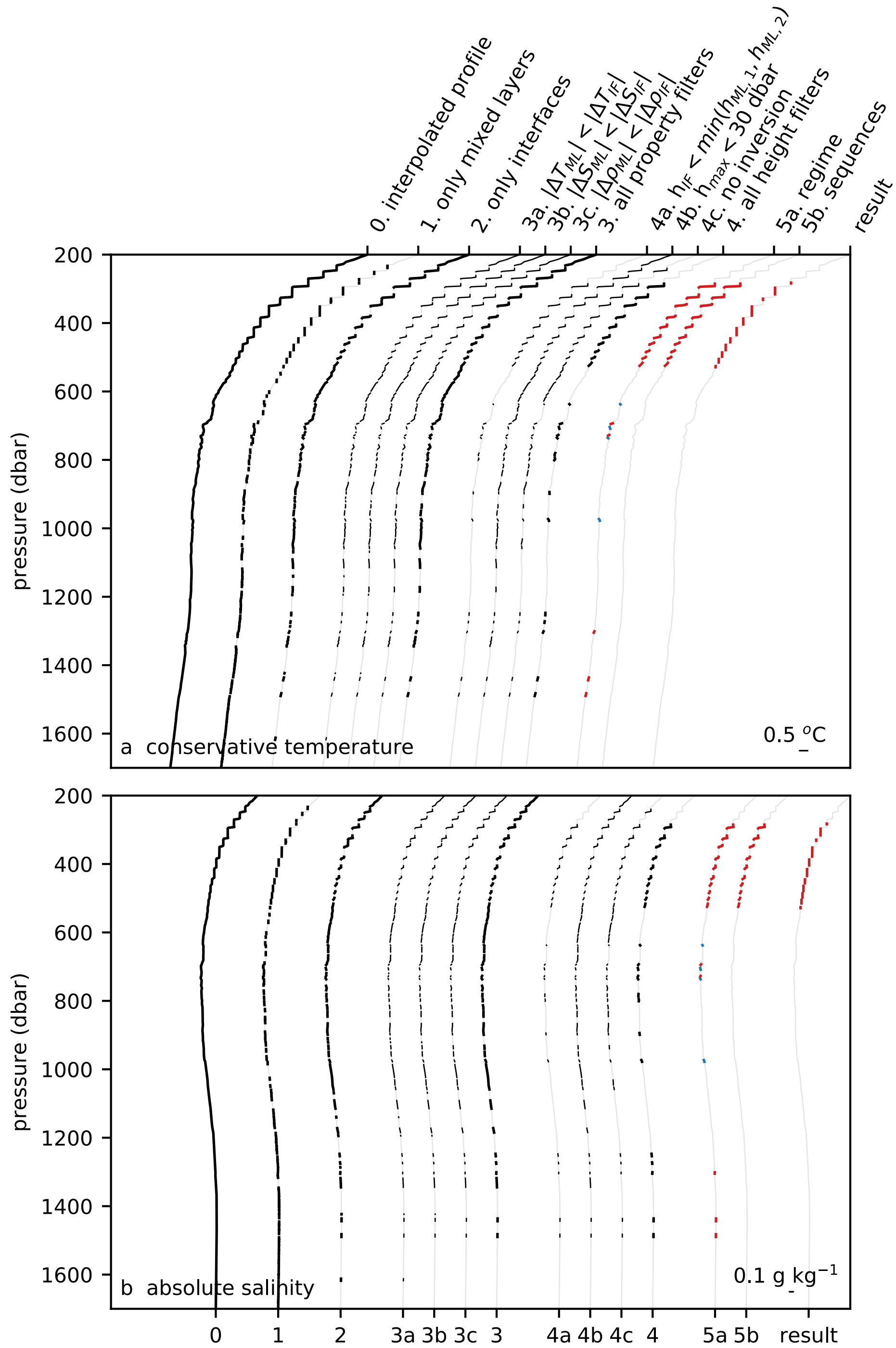

Figure A 6 as Figure A1, but for a profile in the western tropical North Atlantic. Original profile is taken from Argo float 4901478 at 53.3°W and 11.6°N on 9 August 2014.

Figure A2 Structure of the software. Each step in the software is shown by a box. Whenever a particular step is contained inside a function, the name of the function is mentioned above the step. Details of the preprocessing of the data and the detection algorithm are discussed in Sections 2 and Section 3, respectively.

Global dataset of thermohaline staircases obtained from Argo floats and ~~Ice Tethered~~ Ice-Tethered Profilers

Carine G. van der Boog[1], J. Otto Koetsier[1], Henk A. Dijkstra[2], Julie D. Pietrzak[1], and Caroline A. Katsman[1]

[1]Environmental Fluid Mechanics, Civil Engineering and Geosciences, Delft University of Technology, Delft, the Netherlands
[2]Institute for Marine and Atmospheric research Utrecht, Utrecht University, Utrecht, the Netherlands

Correspondence: Carine van der Boog (c.g.vanderboog@tudelft.nl)

Abstract. Thermohaline staircases ~~arise from double diffusive processes~~are associated with double-diffusive mixing. They are characterised by stepped structures consisting of mixed layers of typically tens of meters thick that are separated by much thinner ~~gradient layers~~interfaces. Through these ~~gradient layers~~ interfaces enhanced diapycnal salt and heat transport take place. In this study, we present a global dataset of thermohaline staircases derived from observations of Argo profiling floats and ~~Ice Tethered~~ Ice-Tethered Profilers using a novel detection algorithm. To establish the presence of ~~stepped~~ thermohaline staircases, the algorithm detects subsurface mixed layers and analyses the ~~gradient layers~~ interfaces in between. Of each detected staircase, the ~~temperature,~~ conservative temperature, absolute salinity, depth and height, as well as some other properties of the mixed layers and ~~gradient layers~~ interfaces are computed. The algorithm is applied to 487,~~647~~ 493 quality-controlled temperature and salinity profiles to obtain ~~the~~ a global dataset. The performance of the algorithm is verified through an analysis of independent regional observations. The algorithm and global dataset are available at ~~the 4TU centre for research data (van der Boog et al. (2020b), doi:)~~https://doi.org/10.5281/zenodo.4286170.

1 Introduction

Thermohaline staircases consist of subsurface mixed layers that are separated by ~~gradient layers. They arise from double diffusive~~ thin interfaces. They are associated with double-diffusive processes, which in turn result from a two orders ~~in~~ of magnitude difference between the molecular diffusivity of heat and that of salt (Stern, 1960). Whenever the vertical gradients of temperature- and salinity-induced stratification have the same sign, these differences in molecular diffusivity can enhance the vertical mixing through ~~double diffusive~~ double-diffusive convection, leading to effective diffusivities ~~in~~ of the order of 10^{-4} m^{-2} s^{-1} ~~and the~~ (Radko, 2013, and references therein).

It is still a topic of discussion how double-diffusive convection leads to the formation of thermohaline staircases in oceanic environments (Merryfield, 2000). For example, Stern (1969) argued that small-scale mixing processes trigger the formation of internal waves. On the other hand, variations in the turbulent heat and salt fluxes (Radko, 2003) or in the counter-gradient buoyancy fluxes that sharpen density gradients (Schmitt, 1994) could also lead to the formation of thermohaline staircases~~(Radko, 2013, and~~ ~~.~~. Lastly, subsurface mixed layers can also arise from thermohaline intrusions (Merryfield, 2000). Although it remains unclear how these staircases arise, these studies agree that the formation of these subsurface mixed layers are related to double-diffusive processes.

Based on the ~~the~~ Turner angle (Tu), which compares the density component of the temperature distribution with the density component of the salinity distribution, two regimes of double diffusion can be distinguished (Ruddick, 1983). Waters with $-90° < Tu < -45°$ correspond to a stratification where both temperature and salinity increase with depth and belong to the diffusive-convective regime (DC). Those with $45° < Tu < 90°$ correspond to a stratification where temperature and salinity decrease with depth and belong to the salt-finger regime (SF).

Theoretical and laboratory studies have indicated that diapycnal fluxes of heat and salt in thermohaline staircases are elevated compared to the background turbulence (e.g., Schmitt, 1981; Kelley, 1990; Radko and Smith, 2012; Garaud, 2018). These results were confirmed by a tracer release experiment in the western tropical Atlantic Ocean (Schmitt, 2005). Although these enhanced fluxes were observed, the importance of these fluxes for the global mechanical energy budget remain unknown.

~~Besides the enhanced mixing~~Moreover, the vertical heat and salt fluxes in thermohaline staircases can ~~affect water mass~~ also affect water-mass properties. In some regions, persistent thermohaline staircases with layers stretching ~~horizontally~~ over a few hundred kilometers have been observed (Schmitt et al., 1987; Timmermans et al., 2008; Shibley et al., 2017), which ~~results~~ could result in significant diapycnal fluxes between water masses. For example, the ~~double diffusive~~ double-diffusive diapycnal fluxes in the Mediterranean Sea dominate the transport between the deep water masses (Zodiatis and Gasparini, 1996; Bryden et al., 2014; Schroeder et al., 2016), and in the Arctic Ocean and Southern Ocean, ~~double diffusion regulates sea-ice formation~~ an upward heat flux has been observed through staircase interfaces (Timmermans et al., 2008; Shibley et al., 2017; Polyakov et al., 2012; Bebieva and Speer, 2019).

Modelling studies that incorporated parameterizations of ~~double diffusive~~ double-diffusive fluxes, indicated that the associated double-diffusive diapycnal fluxes ~~have global implications~~ can reduce the strength of the global overturning circulation (Gargett and Holloway, 1992; Merryfield et al., 1999; Oschlies et al., 2003). To ~~study these implications~~be able to study this with observations, we present ~~here~~ a global dataset of the occurrence of thermohaline staircases and their properties. The dataset is based on observations from Argo floats and ~~Ice Tethered~~ Ice-Tethered Profilers. In the following sections we briefly describe the raw data used to extract the dataset (Section 2) and the algorithm we designed to detect staircase structures (Section 3). The sensitivity of this detection algorithm to the chosen input parameters is assessed in Section 4. The dataset is verified in Section 5, followed by some guidelines for the use of the dataset in Section 6.

2 Data ~~pre-processing~~preparation

The dataset contains observations of autonomous Argo floats and autonomous ~~Ice Tethered~~ Ice-Tethered Profilers (ITP). The data of all active and inactive profilers is obtained from http://www.argo.ucsd.edu and http://www.whoi.edu/itp ~~(on~~ from 13 November 2001 to 14 May ~~2020).~~ 2020. Details on the profilers are described in Krishfield et al. (2008) and Toole et al.

Table 1. Number of floats and profiles in the global dataset. Profiles taken with Argo floats are categorised by the Data Assembly Center (DAC). Profiles taken with Ice-Tethered Profilers are categorised as ITP. The percentage between brackets indicates the relative contribution to the total number of profiles in the global dataset (487,493 profiles). More details on abbreviations of DAC can be found in Argo (2019)

DAC / ITP	number of floats	profiles
aoml	2,692	312,285 (64.1 %)
bodc	93	11,092 (2.3 %)
coriolis	347	27,134 (5.6 %)
csio	81	15,099 (3.1 %)
csiro	378	42,942 (8.8 %)
incois	65	4,363 (0.9 %)
jma	205	22,919 (4.7 %)
kma	1	1 (0.0 %)
kordi	0	0 (0.0 %)
meds	145	9,285 (1.9 %)
nmdis	0	0 (0.0 %)
ITP	82	42,373 (8.7 %)

(2011) for the ITP and in Argo (2020) for the Argo floats. First a quality check is performed~~to ensure the quality of the temperature and salinity profiles analysed. A .~~, where a profile is excluded from analysis if it was taken by an Argo float mentioned on the grey list. This grey list contains floats that may have problems with at least one of the sensors (https://www.nodc.noaa.gov/argo/grey_floats.htm). As thermohaline staircases consist of mixed layers with depths of tens of meters, we also require that profiles have continuous data up to 500 dbar with an average resolution finer than 5 dbar. Details on the origin and vertical resolution of the profiles are depicted in Table 1 and Figure 1, in which Figure 1b confirms that all profiles have observations deeper than 500 dbar. Furthermore, the average vertical resolution of the profiles indicates the average resolution is well below the 5 dbar that was used as a threshold (Fig. 1c). After this quality control, 487,~~647~~ 493 vertical temperature and salinity profiles remain. Their global distribution is shown in Figure 2.

Next, ~~all profiles are~~ the profiles of the Argo floats and ITP were linearly interpolated to a vertical resolution of 1 dbar from the surface to 2000 dbar ~~.~~ so that their data could be analysed in a consistent manner. As a result, the small steps in, for example, Arctic staircases might be missed (see Section 5). From these interpolated profiles we calculate several variables. Absolute salinity (S) in g kg^{-1} and conservative temperature (T) in °C are computed with the TEOS-10 software (McDougall and Barker, 2011). ~~We applied~~ Note that we use conservative temperature as this is more accurate than potential temperature in computations concerning heat fluxes and heat content (Graham and McDougall, 2013). We apply a moving average of 200 dbar (Table 2) to obtain the background ~~temperature and~~ conservative temperature and absolute salinity profiles of the water column ~~($\bar{T}$ and $\bar{S}$, respectively) and~~ and to compute the thermal expansion coefficient (α in °C^{-1}) and the haline contraction coefficient (β in kg g^{-1}). A consequence of the moving average of 200 dbar is that the upper 100 dbar and lower 100 dbar

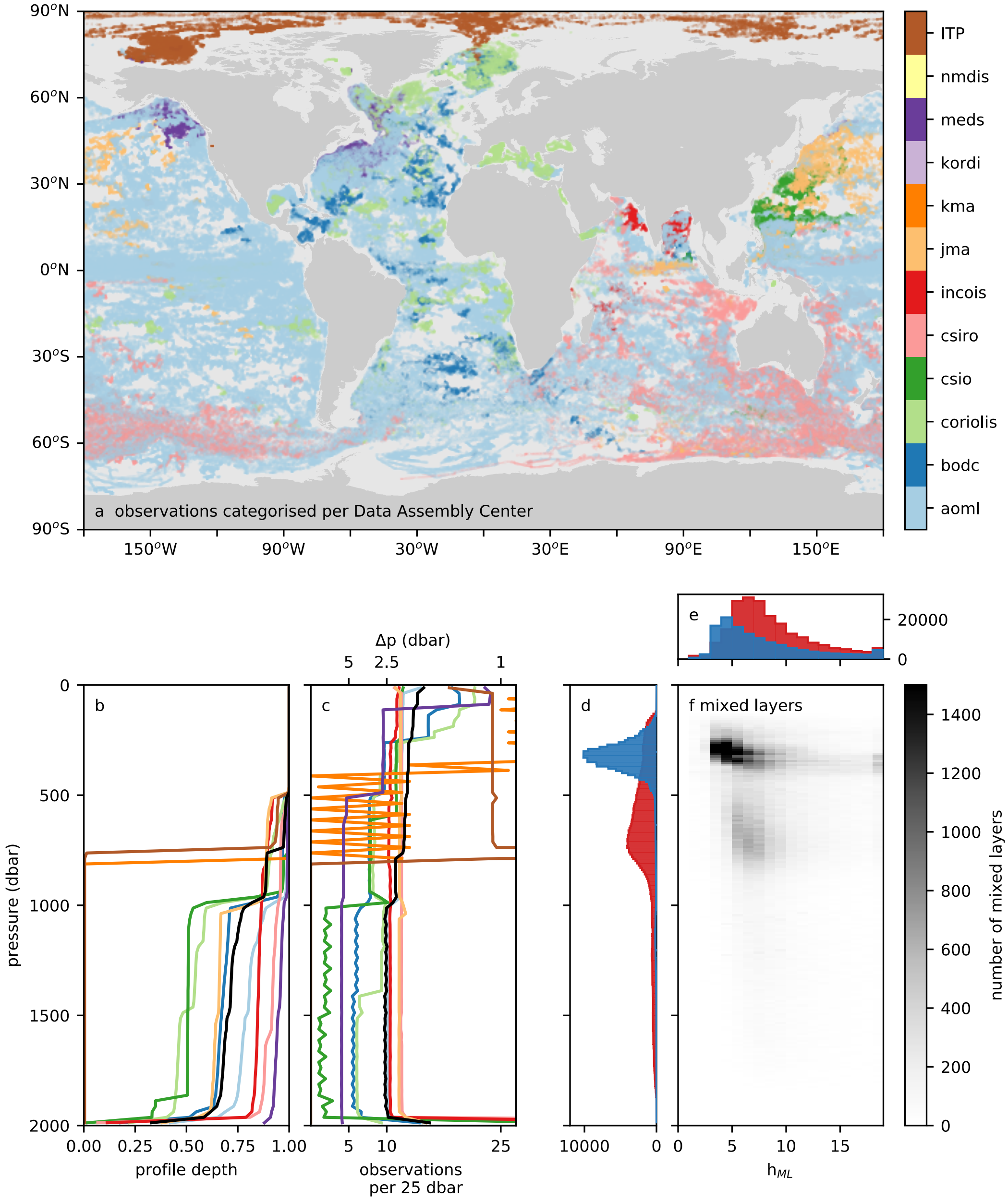

Figure 1. (a) Locations of observations categorised by Data Assembly Centers (DAC) when obtained by an Argo float. Profiles obtained with Ice-Tethered Profilers are indicated with ITP. (b) Cumulative fraction of profiles that reached a given pressure in 25-dbar intervals from 0 to 2,000 dbar per DAC. (c) Average number of observations in 25-dbar intervals from 0 to 2,000 dbar. (d) Distribution of detected mixed layer pressures in the salt-finger (red histogram) or diffusive-convective (blue histogram) regime. (e) Number of detected mixed layers height in the salt-finger (red histogram) or diffusive-convective (blue histogram) regime. (f) Distribution of detected mixed layer heights in thermohaline staircases per pressure level. Panels (b) and (c) were obtained following Wong et al. (2020). Black lines indicate the averages in total global dataset. More details on abbreviations of DAC can be found in Argo (2019)

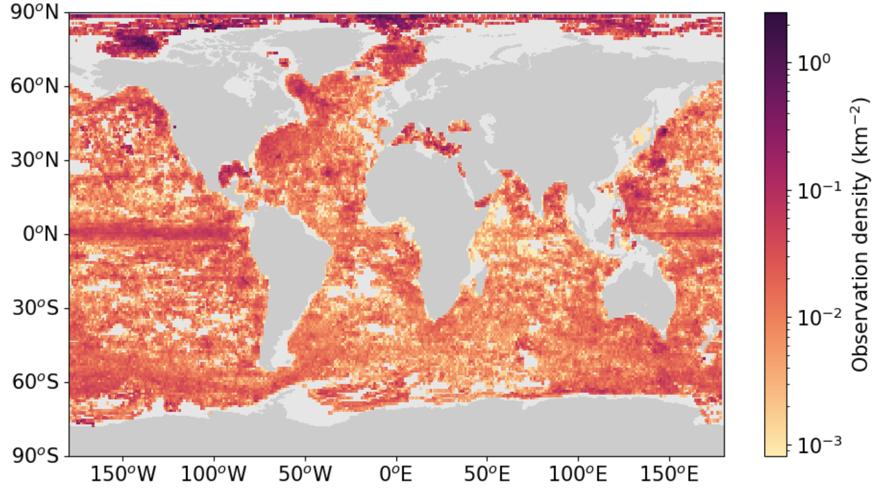

Figure 2. Observation density of the number of profiles obtained from the Argo floats and ~~Ice Tethered~~ Ice-Tethered Profilers after quality control (in km^{-2}). Observation density is binned per degree longitude and degree latitude. Empty bins indicate that no data was available at that location.

Table 2. Input parameters applied during the data ~~pre-processing~~ preparation and the algorithm as used in this study. The sensitivity of the output of the algorithm to the input variables is discussed in the Section 4.

parameter	description	value
moving average window	chosen to obtain background profiles	200 dbar
$\partial\sigma_1/\partial p_{max}$	density gradient threshold for detection mixed layer	0.0005 kg m^{-3} dbar^{-1}
$\Delta\sigma_{1,ML,max}$	maximum density gradient within mixed layer	0.005 kg m^{-3}
$\cancel{h_{GL,max}}$ $h_{IF,max}$	maximum ~~gradient layer~~ interface height	30 dbar

of each profile is omitted in the remainder of the analysis. The Turner angle is computed using ~~smoothed profiles~~ profiles that were smoothed with a moving average of 50 dbar instead of 200 dbar, which is similar to Shibley et al. (2017), following Ruddick (1983), from

$$Tu = \tan^{-1}\left(\alpha\frac{\partial\overline{T}}{\partial p}\frac{\partial T}{\partial p} - \beta\frac{\partial\overline{S}}{\partial p}\frac{\partial S}{\partial p}, \alpha\frac{\partial\overline{T}}{\partial p}\frac{\partial T}{\partial p} + \beta\frac{\partial\overline{S}}{\partial p}\frac{\partial S}{\partial p}\right), \tag{1}$$

where the vertical gradients are approximated with a central differences scheme.

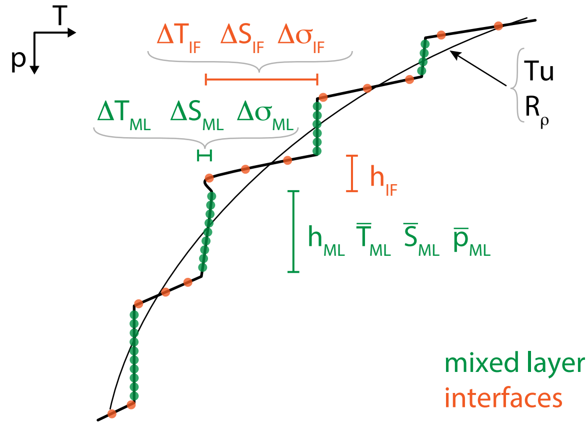

Figure 3. Schematic of a typical temperature profile with staircases, indicating the definitions of the quantities used to detect the thermohaline staircases (green: mixed layer; orange: ~~gradient layer~~interface).

3 Detection algorithm

After the data pre-processing, we apply a detection algorithm that exploits the vertical structure of staircase profiles (Fig. 3). The benefit of using the vertical structure, instead of using assumptions based on the Turner angle, is that we can use this angle to verify the results. The detection algorithm consists of five steps. First the algorithm detects all data points that are located in the subsurface mixed layers (ML, green dots in Fig. 3) by identifying weak vertical density gradients in ~~*T* and *S*~~conservative temperature and absolute salinity. Next, the ~~layer between these~~ properties of any layer lying between the mixed layers (the ~~gradient layers, GL~~interfaces, IF, orange dots in Fig. 3) ~~is~~ are assessed by applying a minimum in temperature and salinity variations. Third, the height of the ~~gradient layer~~ interface and variations within the ~~gradient layer~~ interface are limited. The fourth step determines the regime of double diffusion (diffusive convection or salt fingers), and the fifth step is the identification of sequences of ~~gradient layers~~interfaces, which eventually characterises the thermohaline staircases. The different steps of the algorithm applied to three example profiles are shown in Figures A1-A3. In the following subsections, each algorithm step is described in more detail.

3.1 Mixed layers

The first step of the detection algorithm is the identification of the mixed layers. Preferably, this is done by assessing a density difference relative to a reference pressure, which is the most reliable method to detect a mixed layer (Holte et al., 2017). However, in the case of a thermohaline staircase it is necessary to detect subsurface mixed layers~~where~~ , because the reference pressure is unknown beforehand. To determine this reference pressure, a threshold gradient criterium is applied first (Dong et al., 2008). In this criterium, vertical density gradients are identified as a mixed layer whenever the gradients are below a certain threshold.

We apply the gradient criterium on the vertical gradients of the potential density anomaly at a reference pressure of 1000 dbar (σ_1). We used a threshold of $\partial\sigma_1/\partial p_{max}$ =0.0005 kg m^{-3} dbar^{-1} (Table 2), which is similar to mixed layer gradients used by Bryden et al. (2014). Furthermore, this threshold gradient is ~~well above~~ slightly larger than the threshold used by Timmermans et al. (2008), who used 0.005°C m^{-1} (which corresponds to $\partial\sigma_1/\partial p_{max}$ =0.00036 kg m^{-3} dbar^{-1}). The threshold gradient method is applied on both ~~temperature and~~ conservative temperature and absolute salinity profiles, i.e.,

$$\left|\alpha\rho_0\frac{\partial T}{\partial p}\right| \leq 0.0005 \text{ kg m}^{-3}\text{dbar}^{-1},$$
$$\left|\beta\rho_0\frac{\partial S}{\partial p}\right| \leq 0.0005 \text{ kg m}^{-3}\text{dbar}^{-1}. \tag{2}$$

Also the vertical density gradients from the combined temperature and salinity effects must satisfy this condition:

$$\left|\frac{\partial\sigma_1}{\partial p}\right| \leq 0.0005 \text{ kg m}^{-3}\text{dbar}^{-1}. \tag{3}$$

These three conditions ensure that the vertical ~~temperature, salinity and~~ conservative temperature, absolute salinity and potential density gradients are all below the threshold value. At each pressure level where all three conditions are met the datapoint is identified as a mixed layer. Next, for each continuous sequence of ~~datapoints~~data points, the algorithm computes the average pressure. This is then used as a reference pressure, which is required to be able to apply the mixed layer detection.

At every reference pressure, a maximum density range is required within the mixed layers to identify the full vertical extent of each mixed layer. To allow for small variations of ~~temperature and~~ conservative temperature and absolute salinity in the mixed layer, but to exclude variations in the ~~gradient layer~~interface, we use a threshold of $\Delta\sigma_{1,ML,max}$ =0.005 kg m^{-3} for density variations within each mixed layer (Table 2). This density range corresponds to the density range used by Holte et al. (2017) for the detection of surface mixed layers. The applied density range allows for mixed layers with heights ~~in~~ of the order of 10 m assuming gradients of $\partial\sigma_1/\partial p_{max}$ =0.0005 kg m^{-3} dbar^{-1}. To ensure separation between individual mixed layers, the upper and lower datapoint of each mixed layer are removed. Note that this results in a minimum ~~gradient layer~~ interface height of 2 dbar~~.~~ , which could result in false negatives in for example the Arctic Ocean (Section 5).

After applying the threshold for density range, the algorithm defines each continuous set of datapoints as a mixed layer and computes the average pressure ($\overline{p}_{ML}$), average conservative temperature ($\overline{T}_{ML}$), average absolute salinity ($\overline{S}_{ML}$), mixed layer density ratio ($\overline{R}_\rho = \alpha\frac{\partial\overline{T}}{\partial p}/\left(\beta\frac{\partial\overline{S}}{\partial p}\right)$), average Turner angle ($\overline{Tu}_{ML}$) and height (h_{ML}) for each mixed layer.

3.2 ~~Gradient layers~~Interfaces: conservative temperature and absolute salinity variations

The algorithm defines ~~a gradient layer~~ an interface as the part of the water column between two mixed layers. In addition, to ensure a stepped structure the algorithm requires that the ~~temperature, salinity and~~ conservative temperature, absolute salinity and potential density variations within each mixed layer should be smaller than the variations in the ~~gradient layer~~ interface

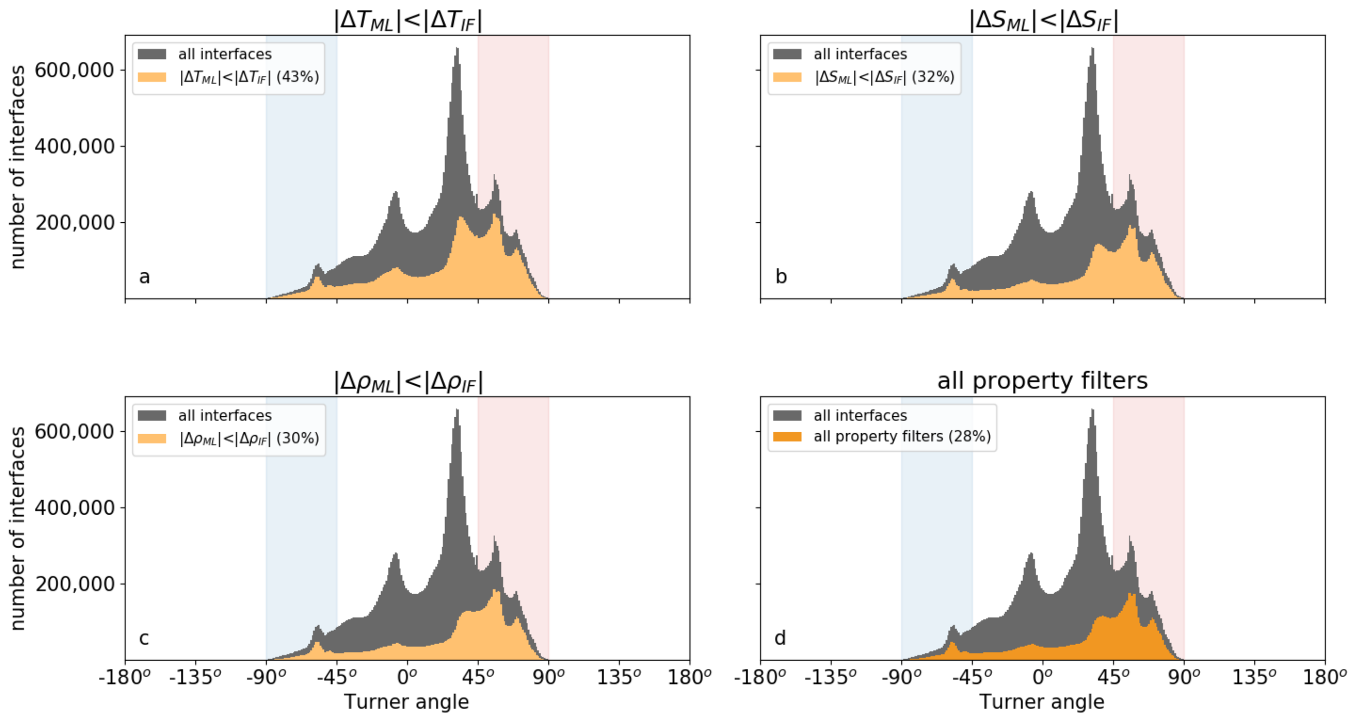

Figure 4. Histogram of the number of detected ~~gradient layers~~ interfaces as a function of the Turner angle (Tu) by applying a criteria for (a) conservative temperature, (b) absolute salinity, (c) potential density and (d) all three properties given in equation 4 (orange shading). Each panel shows the data remaining compared to the raw ~~gradient layer~~ interface data (grey). Vertical shaded bands correspond to Turner angles in the diffusive-convective (blue) and salt-finger (red) regime.

(Fig. 3):

$$
\begin{aligned}
\max\left(|\Delta T_{ML,1}|,|\Delta T_{ML,2}|\right) &< |\Delta T_{IF}|;\\
\max\left(|\Delta S_{ML,1}|,|\Delta S_{ML,2}|\right) &< |\Delta S_{IF}|;\\
\max\left(|\Delta \sigma_{1,ML,1}|,|\Delta \sigma_{1,ML,2}|\right) &< |\Delta \sigma_{1,IF}|;
\end{aligned}
\tag{4}
$$

where the subscripts 1 and 2 correspond to the mixed layer directly above and below ~~a gradient layer~~an interface, respectively. It appears that most data points that meet these requirements (orange histograms in Fig. 4a-c) have Turner angles in the two ~~double diffusive~~ double-diffusive regimes. This dependence of the variations in the ~~gradient layers~~ interfaces on the Turner angle is in line with expectations that staircase-like structures are mostly found within ~~double diffusive~~ double-diffusive regimes. In total, 28 % of all detected ~~gradient layers~~ interfaces meet all three requirements (Fig. 4d).

3.3 ~~Gradient layer~~Interface: height

The next step in the staircase detection algorithm is to limit the height of the ~~gradient layer (Fig. 3)~~ interface to ensure that the mixed layers are separated from each other by a relatively thin ~~gradient layer. We require~~ interface (Fig. 3). We require

$$h_{\cancel{GL}IF} < \min\left(h_{ML,1}, h_{ML,2}\right), \tag{5}$$

i.e. the ~~gradient layer~~ interface height is smaller than the height of the mixed layers directly above and below the ~~gradient layer~~interface. In total, 27 % of the ~~gradient layers~~ interfaces that fulfilled the ~~temperature and~~ conservative temperature and absolute salinity requirements meet this requirement (Fig. 5a). Note that this part of the algorithm defines the top and bottom of a sequence of a staircase in a profile. ~~However, it appears that this height requirement is not sufficient everywhere. For example, in the Mediterranean Sea thermohaline staircases exist with mixed layers over 100 m and gradient layers of 20 m (Zodiatis and Gasparini, 1996; Radko, 2013). To prevent the false detection of large vertical gradient layers of up to hundreds of meters in profiles with such thick mixed layers, we limit the gradient layer height to $h_{GL,max}$ =30 dbar (Table 2). This only affects the classification of 1 % of the gradient layers (Fig. 5b).~~

Furthermore, the tallest observed ~~gradient layers~~ interfaces are found in the Mediterranean Sea with heights up to ~~h_{GL} =20~~ h_{IF} =27 m, where they separate mixed layers of over 100 m (Zodiatis and Gasparini, 1996; Radko, 2013). To prevent false detection of large vertical ~~gradient layers~~ interfaces of up to hundreds of meters, we limit the ~~gradient layer height to $h_{GL,max}$ =~~interface height to $h_{IF,max}$ =30 dbar (Table 2, Fig. 5b). This only affects the classification of 1 % of the interfaces (Fig. 5b).

To solely detect step-like ~~profiles~~ structures that are associated with the presence of thermohaline staircases, the algorithm also removes all ~~gradient layers with temperature or salinity inversions~~ interfaces with conservative temperature or absolute salinity inversions. This is done by limiting the number of local minima and maxima of the ~~temperature and~~ conservative temperature and absolute salinity allowed in each ~~gradient layer~~ interface to two (Fig. 5c). The combination of all three ~~gradient layer~~ interface height requirements is met by 27 % of the ~~gradient layers~~ interfaces detected based on the ~~temperature and~~ conservative temperature and absolute salinity requirements discussed in the previous section (Fig. 5d).

3.4 ~~Gradient layer~~Interface: ~~double diffusive~~ double-diffusive regime

After the algorithm has selected all the ~~gradient layers~~ interfaces with a step-like structure, the ~~double diffusive~~ double-diffusive regime of each ~~gradient layer~~ interface is assessed (Fig. 6a). In case both ~~temperature and~~ conservative temperature and absolute salinity of the mixed layers above and below the ~~gradient layer~~ interface increase with pressure, the ~~gradient layer~~ interface is classified as the diffusive-convective regime. If the ~~mixed layer temperature and salinity~~ conservative temperature and absolute salinity of the mixed layers above and below the interface both decrease with ~~depth, the gradient layer~~ pressure, the interface belongs to the salt-finger regime. The algorithm detects more ~~gradient layers~~ interfaces in the salt-finger regime (27 %) than in the diffusive-convective regime (11 %, Fig. 6a).

~~Most gradient layers are found in the salt-finger regime (27%).~~ As expected, most ~~gradient layers~~ interfaces with diffusive-convective characteristics have ~~Tu values~~ Turner angles between $-90° < Tu < -45°$ (blue histogram in Fig. 6a) and most

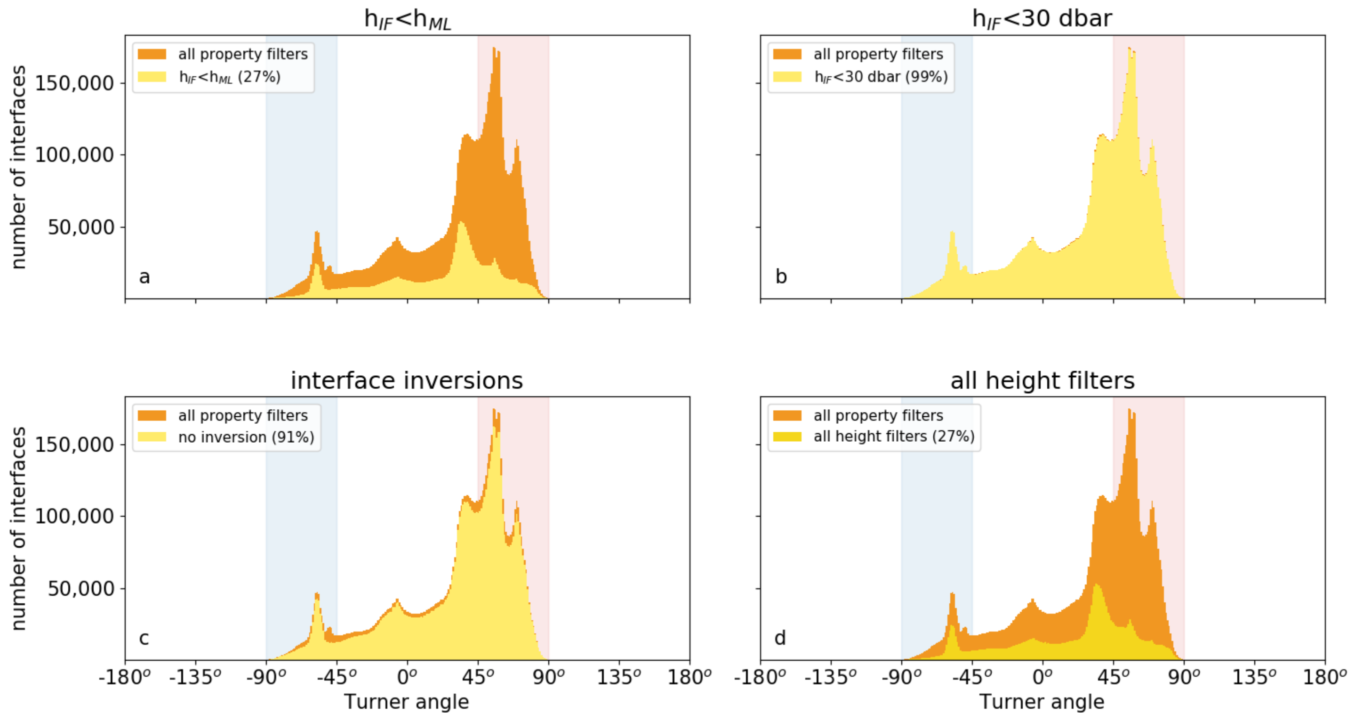

Figure 5. Histogram of the number of detected ~~gradient layers~~ interfaces as a function of the Turner angle (Tu) by applying a criteria for (a) height, (b) maximum height, (c) inversions and (d) all three height limitations (yellow shading). Each panel shows the data remaining compared to the ~~gradient layers~~ interfaces detected based on the conservative temperature and absolute salinity requirements shown in Fig. 4d (orange shading). Vertical shaded bands correspond to Turner angles in the diffusive-convective (blue) and salt-finger (red) regime.

salt-finger ~~gradient layers have Tu values~~ interfaces have Turner angles between $45° < Tu < 90°$ (red histogram in Fig. 6a). This implies that these ~~gradient layers~~ interface properties are consistent with the background stratification.

3.5 Sequences of ~~gradient layers~~interfaces

The final step of the detection algorithm is to only select vertical sequences of at least two ~~gradient layers~~ interfaces in the same ~~double diffusive regime~~ double-diffusive regime that are separated from each other by one mixed layer (Fig. 6b). This step removes most thermohaline intrusions, as these are characterized by alternating mixed layers in the diffusive-convective and salt-finger regime (Bebieva and Timmermans, 2017). In this final step, the algorithm also removes also salt-finger ~~gradient layers~~ interfaces and diffusive-convective ~~gradient layers~~ interfaces outside their favourable Turner angle (compare Fig. 6a and Fig. 6b).

After applying ~~the entire~~ this final step of the algorithm, we obtain a global dataset consisting of 166,~~143 gradient layers~~ 141 interfaces in the salt-finger regime and 119,619 ~~gradient layers in~~ interfaces in the diffusive-convective regime. The distribution

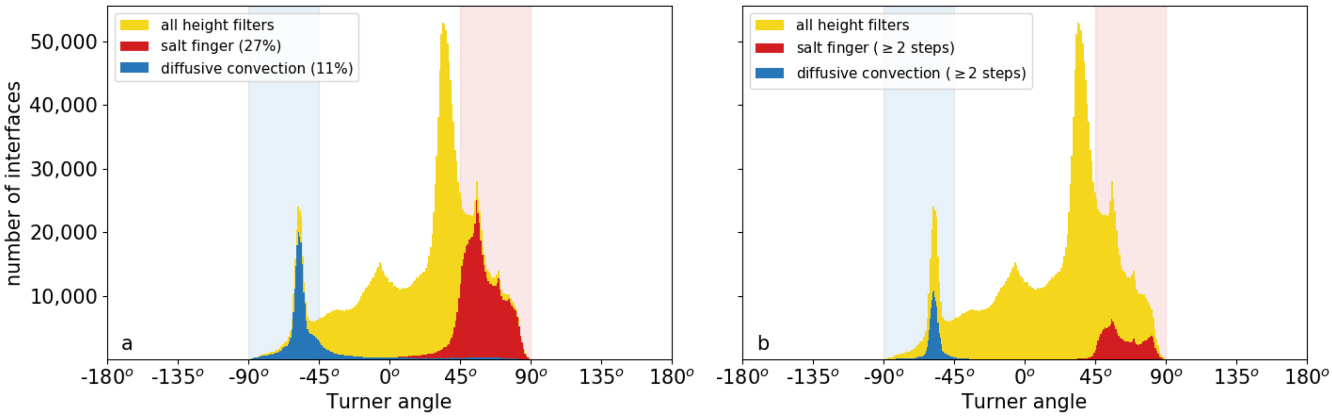

Figure 6. Histogram of the number of detected ~~gradient layers~~ interfaces as a function of the Turner angle (Tu) after (a) classification of the ~~double diffusive~~ double-diffusive regime and (b) selection of sequences of the ~~gradient layers~~interfaces. Each panel shows the data remaining compared to the ~~gradient layers~~ interfaces detected based ~~gradient layer~~ interface height requirement shown in Fig. 5d (yellow shading). Vertical shaded bands correspond to Turner angles in the diffusive-convective (blue) and salt-finger (red) regime.

of the pressure levels and height of the mixed layers at these interfaces is displayed in Fig. 1. In general, mixed layers in the diffusive-convective regime ~~. Some examples thermohaline staircases~~are found at lower pressure levels than mixed layers in the salt-finger regime (Fig. 1d). At the same time, the height of the mixed layers in the diffusive-convective regime are smaller, which is in line with previous observations (Fig. 1e, e.g., Radko, 2013). Recall that the algorithm required a minimal interface height of 2 dbar, which implies that, following equation 5, the minimal mixed layer height is 3 dbar and that the detection of interfaces is cut off below these limits. Consequently, the interfaces with smaller heights are missed by the algorithm. Figure 1e indicates that this is more problematic for interfaces in the diffusive-convective regime than for interfaces in the salt-finger regime.

Examples of thermohaline staircases, which were selected based on their high number of interfaces, are shown in Figure 7. In line with ~~expectations~~previous results (Rudels, 2015), staircases in the diffusive-convective regime (Fig. 7a) are mainly detected on the thermocline with ~~temperatures~~ the conservative temperature increasing with depth. ~~Thermohaline staircases~~ These staircases are predominantly located in the Arctic Ocean at a depth between 300-400 m, which is between the warm and saline Atlantic Water and cold and fresh surface waters (Rudels, 2015). Figure 7a also indicates that the deepest mixed layer of some thermohaline staircases is located at the temperature maximum, which suggests that this lowest layer might be the result of thermohaline intrusions (Ruddick and Kerr, 2003). There, the algorithm identified a mixed layer, because temperature and salinity stratification were weak enough (see Section 3.1). Furthermore, both conservative temperature and absolute salinity in this mixed layer are larger than in the mixed layer above. While both are typical for a staircase in the diffusive-convective regime, the algorithm does not detect whether this mixed layer is a temperature maximum, which could indicate that arose from thermohaline intrusions. Note that this only concerns the deepest mixed layers of the staircases, and that only the characteristics of the interfaces in between mixed layers are labelled as part of a staircase by the algorithm.

Thermohaline staircases with a high number of steps in the salt-finger regime are detected ~~where the~~ on the main thermocline where the conservative temperature decreases with depth (Fig. 7b). Compared to the staircases in the diffusive-convective regime, these staircases are located slightly deeper at 400-700 m. While the locations of these staircases vary, they are located above the cold and fresh Antarctic Intermediate Water, which is observed below 700 m (Tsuchiya, 1989; Fine, 1993; Talley, 1996) .

For each thermohaline staircase, characteristics of the ~~gradient layers~~ interfaces and mixed layers, such as their ~~temperature,~~ conservative temperature, absolute salinity and height, are available in the dataset. An overview of the provided variables is given in Table A1. The detection algorithm is verified by comparing our data to independent observations in three regions in Section 5.

~~Example temperature profiles selected by the staircase detection algorithm. They are ordered left-right by the number of steps detected. Top panel shows examples of increasing steps of diffusive convection, bottom panel shows examples of the salt-finger regime.~~

4 Robustness of the detection algorithm

The algorithm requires four input parameters: the moving average window, a threshold for the maximum density gradients of the mixed layers, the maximum density difference of the mixed layers and the maximum height of the ~~gradient layer~~interface (Table 2). In this section, the sensitivity of the algorithm to each input parameter is assessed (Fig. 8).

The moving average window is used by the algorithm to compute the thermal expansion coefficient (α), the haline contraction coefficient (β) and the density ratio (R_ρ). We varied the moving average window between 50 dbar and 350 dbar to assess the sensitivity of the outcomes of this choice (Fig. 8a). We find that the varying moving average window does not result in large variations in detected mixed layers (Fig. 8a).

In contrast to the ~~moving average~~ moving-average window, the detection algorithm is sensitive to the value set for the density gradient threshold of the mixed layer (Fig. 8b), which is used to obtain a reference pressure for the sub-surface mixed layers (Section ~~3.1~~3.1). Not surprisingly, we detect more (less) ~~gradient layers~~ interfaces when we increase (decrease) the allowed threshold density gradient. A small value allows for only the strongest mixed layers to be detected, which are usually referred to as well-defined staircases, while a large density gradient also allows for the detection of rough staircases (e.g., Durante et al., 2019). Although the number of detected ~~gradient layers~~ interfaces depends on the value set for this density gradient, the detected ~~gradient layers~~ interfaces remain confined to the two double-diffusive regimes, indicating a robust outcome of the algorithm for the choice of this input parameter.

Similar to the variations of the maximum density gradient, the variation of the maximum density difference allowed within the mixed layer results in a different number of detected ~~gradient layers~~ interfaces (Fig. 8c). The number of detected mixed layers increases when we decrease the maximum density difference allowed within the mixed layer. This effect is mostly visible

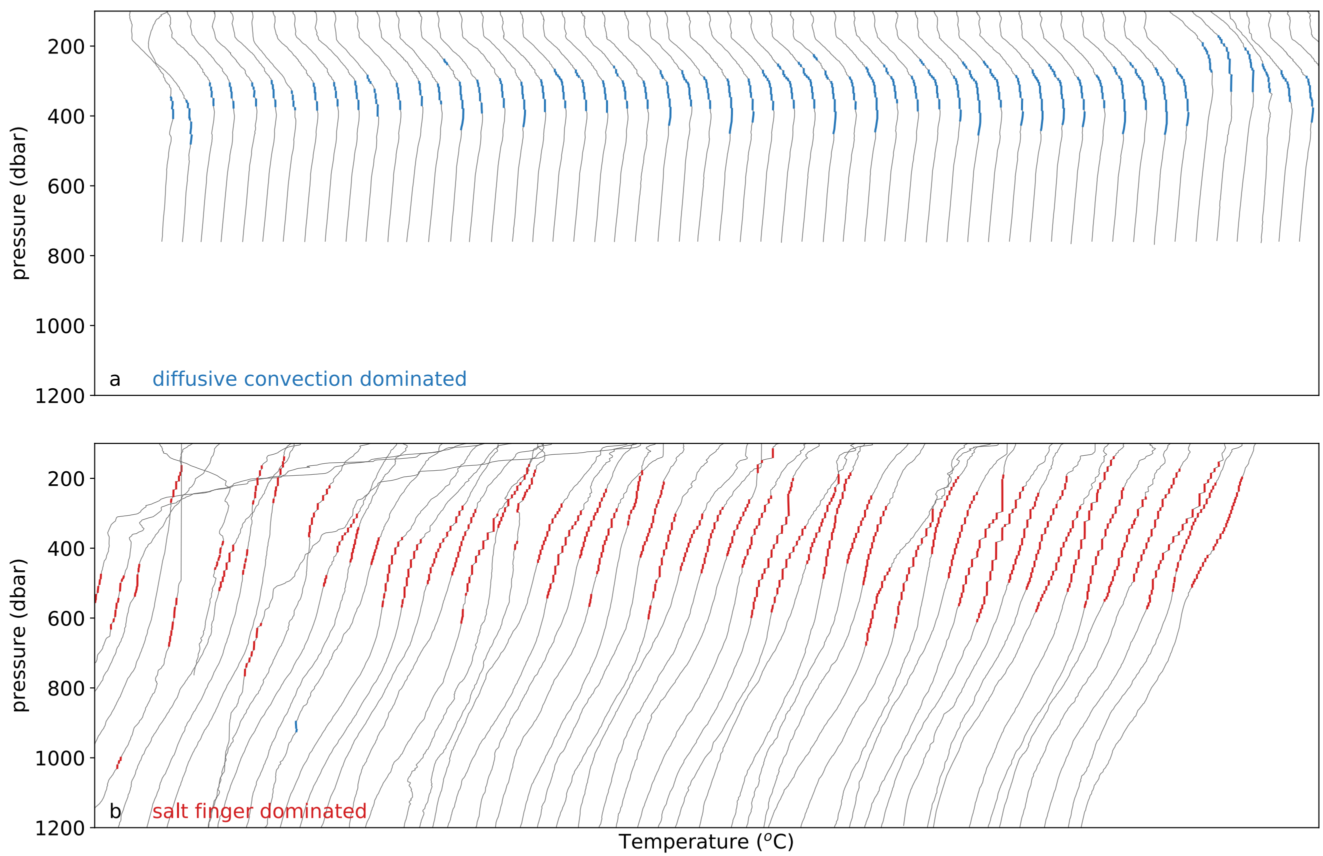

Figure 7. Example conservative temperature profiles selected by the staircase detection algorithm. They are ordered left-right by the number of steps detected. Top panel shows examples of increasing steps of diffusive convection, bottom panel shows examples of the salt-finger regime.

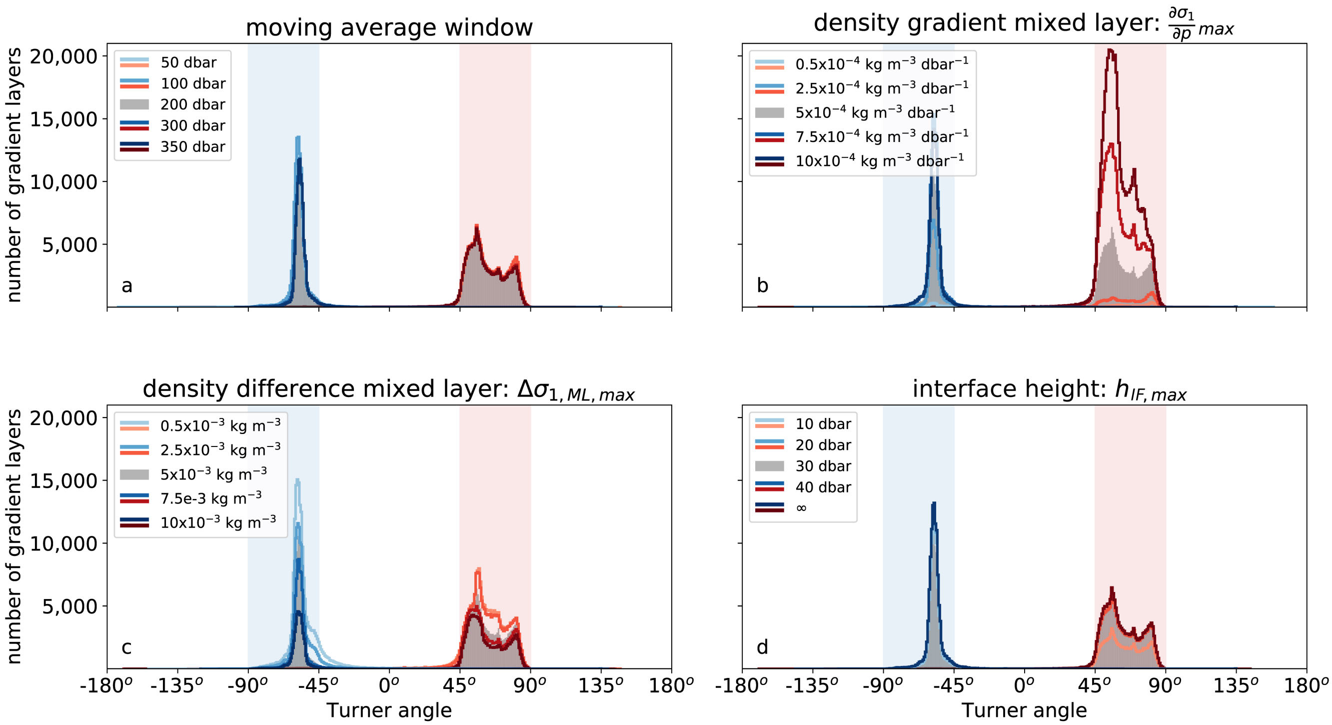

Figure 8. Number of detected ~~gradient layers~~ interfaces obtained with the detection algorithm for different input parameters. Each subpanel shows the sensitivity of the detection algorithm to one input parameter: (a) moving average window, (b) density gradient of the mixed layer, (c) density difference within the mixed layer and (d) the maximum height of the ~~gradient layer~~interface. In each panel, the grey histogram corresponds to the default parameters listed in Table 2. The colored lines correspond to the varying parameter (see legend). Shaded regions indicate Turner angles in the diffusive-convective (blue) and salt-finger (red) regime.

in the diffusive-convective regime, as we obtained a decrease of 54 % of detected ~~gradient layers~~ interfaces in the diffusive-convective regime compared an decrease of 31 % of detected ~~gradient layers~~ interfaces in the salt-finger regime in case we doubled the density difference in the mixed layer ($\Delta\sigma_{1,max} = 10 \times 10^{-3}$ kg m^{-3}). This difference between the regimes is due to relatively small ~~gradient layer~~ interface variations in the diffusive-convective regime compared to the salt-finger regime (Radko, 2013) and can be explained as follows: When a too large density difference is applied, the relatively small density gradients in the ~~gradient layers~~ interfaces of the diffusive-convective regime are detected as mixed layers by the algorithm. Consequently, multiple mixed layers can be identified as a single mixed layer. However, if the applied density difference is too small, this could result in the detection of multiple mixed layers per staircase step.

The last input parameter of the detection algorithm concerns the ~~gradient layer~~ interface height (Fig. 8d). As expected from Fig. 5b, variations of this input parameter do not result in large differences in the number of detected ~~gradient layers~~interfaces. If we omit this input parameter by setting it to infinity, we obtain a total increase of detected ~~gradient layers~~ interfaces of 17 %.

Overall, the detection algorithm gives robust results as it predominantly detects ~~gradient layers~~ interfaces within the double-diffusive regime (Fig. 8). In line with expectations, the detection algorithm is most sensitive to the threshold value for the maximum density gradient in the mixed layer and the density variations within the mixed layers. The four input variables allow for ~~optimalization~~ optimisation of the detection algorithm based on the regime and characteristics of the staircases.

5 Regional verification

The characteristics of thermohaline staircases obtained with the detection algorithm are compared to those obtained from previous observational studies for three major staircase regions: the Canada Basin in the Arctic Ocean, the Mediterranean Sea, and the C-SALT region in the tropical Atlantic Ocean. An overview is given in Tables 3-5.

In the Canada Basin (135°W-145°W, 75°N-80°N), the algorithm detects thermohaline staircases in the diffusive-convective regime in 90 % of the profiles (Table 3). Both the occurrence and depth range are comparable to what was reported by Timmermans et al. (2008) and Shibley et al. (2017), who ~~analysed~~ analyzed thermohaline staircases from several ~~Ice Tethered~~ Ice-Tethered Profilers, demonstrating that our detection algorithm indeed detects thermohaline staircases at the right location. Microstructure observations suggested that the thermohaline staircases in Canada Basin have ~~gradient layers~~ interfaces heights of approximately ~~h_{GL}~~ h_{IF} = 0.15 m (Padman and Dillon, 1987; Radko, 2013). Due to the vertical resolution of the profiles and the design of the algorithm (recall that the mixed layers are separated from each other by removing the upper and lower datapoint of the mixed layer, Section 3.1), ~~it~~ the method is not capable of detecting very thin ~~gradient layers. Despite~~ interfaces (Figure A1). As expected from these limitations for ~~detection gradient layer~~ the detection of the interface heights, the algorithm detects ~~temperature and~~ conservative temperature and absolute salinity steps (~~ΔT_{GL} and ΔS_{GL}~~ ΔT_{IF} and ΔS_{IF}, respectively) in the gradients layers that ~~have a magnitude comparable to~~ are in the upper ranges of earlier observations (Padman and Dillon, 1987; Timmermans et al., 2003, 2008; Shibley et al., 2017).

In the Mediterranean Sea, thermohaline staircases are characterized by relatively thick mixed layers that are separated by thick ~~gradient layers~~ interfaces of up to 27 m (Zodiatis and Gasparini, 1996). In this region (0°E-15°E, 30°N-43°N), the ~~staircase~~ detection algorithm detected thermohaline staircases with ~~gradient layers~~ interfaces up to 21 dbar in 6 % of the profiles, which is comparable to previous observations (Table 4). ~~However, the~~ An example of the detection of a Mediterranean staircase is shown in Figure A2. We find that the depth at which the thermohaline staircases occur is underestimated by the detection algorithm~~, which is due to the limited depth range (mostly~~ . This could be explained by the fact that most Mediterranean observations are obtained by the Coriolis DAC (Fig. 1a). From this DAC, approximately 50 % of the profiles have observations that are deeper than 1000 dbar ~~) of the Argo floats in this region~~(Fig. 1b), which means that the coverage below 1000 dbar is limited in the Mediterranean Sea. Although the Argo floats, and consequently the detection algorithm, do not cover the full extent of the staircases ~~, the temperature and~~ (Fig. 1), the conservative temperature and absolute salinity steps that are found are similar to previous observations (Table 4). Note that the ~~temperature and~~ conservative temperature and absolute salinity steps of the staircases increase with depth (Zodiatis and Gasparini, 1996), which explains why the ~~temperature~~

Table 3. Characteristics of thermohaline staircases in Canada Basin. The region of the global dataset is confined to: 135°W-145°W, 75°N-80°N. The observational techniques indicate if the data was obtained from Argo floats (Argo), ~~Ice Tethered~~ Ice-Tethered Profilers (ITP), Conductivity Temperature Depth measurements (CTD) or microstructure measurements (MS). The dominant type of thermohaline staircases is indicated by DC (diffusive convection) and SF (salt-finger) with the percentage of occurrence between brackets. Ranges of the obtained variables of the global dataset are indicated by means of the 2.5 and 97.5-percentile.

	technique	type	depth range (dbar)	$\cancel{\Delta T_{GL}}$ ΔT_{IF} ($^\circ C$)	$\cancel{\Delta S_{GL}}$ ΔS_{IF} (g kg^{-1})	$\cancel{h_{GL}}$ h_{IF} (dbar)
global dataset	ITP + Argo	DC (90 %)	263 - 448	0.007 - 0.1	0.003 - 0.04	2 - 9
Padman and Dillon (1987)	CTD+MS	DC (100 %)	320 - 430	0.004 - 0.013	0.0016 - 0.0049	0.15
Timmermans et al. (2003)	CTD	DC	2400-2900	0.001 - 0.005	0.0035 - 0.0045	2 - 16
Timmermans et al. (2008)	ITP	DC (96 %)	200 - 300	0.04	0.014	
Shibley et al. (2017)	ITP	DC (80 %)		0.04±0.01	0.01 ±0.003	$<$ 1 m

Table 4. as Table 3, but for the Mediterranean Sea (0°E-15°E, 30°N-43°N).

	technique	type	depth range (dbar)	$\cancel{\Delta T_{GL}}$ ΔT_{IF} ($^\circ C$)	$\cancel{\Delta S_{GL}}$ ΔS_{IF} (g kg^{-1})	$\cancel{h_{GL}}$ h_{IF} (dbar)
global dataset	ITP + Argo	SF (6 %)	287 - 866	0.0097 - 0.12	0.0017 - 0.031	3 - 21
Zodiatis and Gasparini (1996)	CTD	SF	600 - 2500	0.04 - 0.17	0.01 - 0.04	2 - 27
Bryden et al. (2014)	CTD	SF (32 %)	600 - 1400	0.03 - 0.13	0.009 - 0.03	5 - 16
Buffett et al. (2017)	seismic imaging	SF	550 - 1200			
Durante et al. (2019)	CTD	SF	500 - 2500	approx. 0.15		4 -17

~~and~~ conservative temperature and absolute salinity steps detected by the algorithm are slightly smaller than those observed in the deeper observations (Zodiatis and Gasparini, 1996; Durante et al., 2019).

In the C-SALT region in the western tropical North Atlantic Ocean (53°W-58°W, 10°N-15°N), the algorithm detected thermohaline staircases in the salt-finger regime in 60 % of the profiles (Table 5). Similar to previous studies (Schmitt et al., 1987; Schmitt, 2005; Fer et al., 2010), the algorithm detected thermohaline staircases on the main thermocline ~~.~~ (see example in Fig. A3). Again, the ~~gradient layer~~ interface height is slightly overestimated by the detection algorithm, but the algorithm obtained ~~temperature and~~ conservative temperature and absolute salinity steps comparable to previous studies.

Overall, the comparison between the outcomes of the detection algorithm with previous studies indicates that the detection algorithm performs well. The small overestimation of the ~~gradient layer~~ interface height can be attributed to the limited vertical resolution and the limitation imposed by the detection algorithm to avoid detection of false positives. Despite this

Table 5. as Table 3, but for the western tropical North Atlantic Ocean (53°W-58°W, 10°N-15°N).

	technique	type	depth range (dbar)	$\cancel{\Delta T_{GL}}$ ΔT_{IF} ($°C$)	$\cancel{\Delta S_{GL}}$ ΔS_{IF} (g kg^{-1})	$\cancel{h_{GL}}$ h_{IF} (dbar)
global dataset	ITP + Argo	SF (60 %)	265 - 837	0.019 - 0.97	0.0014 - 0.16	3 - 18
Schmitt et al. (1987)	CTD+MS	SF	180 - 650	0.5 - 0.8	0.1 - 0.2 psu	1 - 10
Schmitt (2005)	CTD+MS	SF	200 - 600	<1		0.5 - 5
Fer et al. (2010)	Seismic imaging	SF	550 - 700			

overestimation, the ~~gradient layers~~ interfaces are detected at the correct depths with ~~temperature and~~ conservative temperature and absolute salinity steps within ~~the right range~~realistic ranges. Therefore, we conclude that the detection algorithm is very suitable for the automated detection of thermohaline staircases in large and quickly growing datasets like the Argo float and ~~Ice Tethered~~ Ice-Tethered Profilers data.

6 Conclusions

In this study, we presented an algorithm to automatically detect thermohaline staircases from Argo float profiles and ~~Ice Tethered Profiles. The~~ Ice-Tethered Profiles. As these thermohaline staircases have different mixed layer heights and temperature and salinity steps across the interfaces in different staircase regions, the design of the detection algorithm is based on the typical vertical structure and shape of the staircases (Fig. 3-5). Note that by formulating the algorithm solely on this vertical structure of the staircases, ~~there is no need to make any assumption about their physical properties beforehand. The~~ we could use the Turner angle of the detected staircases ~~indicates~~ for verification. Using this Turner angle, we showed that the structures are within the two ~~double diffusive~~ double-diffusive regimes: the salt-finger regime and the diffusive-convective regime (Fig. 6).

We optimized the input of the algorithm such that it provides a global overview and limits the number of detected false positives. As a result, the regional verification in Section 5 indicated that the data pre-processing and data analysis have some limitations. For example, the vertical resolution of 1 dbar in the profiles is too course to capture all staircase steps in the Arctic Ocean. In the Mediterranean, the Argo floats did not dive deep enough to capture the full depth of the staircase region. However, the fact that (i) the algorithm detects thermohaline staircases at realistic depth ranges, with (ii) conservative temperature and absolute salinity steps across the interfaces, and in (iii) the same double-diffusive regime as previous studies (Table 3-Table 5), indicates that the algorithm itself performs well. Therefore, when considering an individual staircase region, we recommend optimizing the input variables of the algorithm for that specific region and applying the algorithm on additional data, for example high-resolution CTD or microstructure profiles, where available.

A sensitivity analysis to different input parameters showed that the results of the detection algorithm are robust; the detected staircase ~~gradient layers~~ interfaces are confined to the ~~double diffusive~~ double-diffusive regimes. Furthermore, ~~a~~ the

Table A1. Metadata of all variables that are saved in the dataset.

variable	unit	description
floatID		float identification number of ITP or Argo float
lat	°E	latitude of observation
lon	°N	longitude of observation
juld	days	~~julian~~ Julian date of observation
ct	°C	conservative temperature (full profile)
sa	g kg^{-1}	absolute salinity (full profile)
p_{ML}	dbar	average pressure of the mixed layer
h_{ML}	dbar	height of the mixed layer
T_{ML}	°C	average conservative temperature of mixed layer
S_{ML}	g kg^{-1}	average absolute salinity of mixed layer
Tu_{ML}	°	average Turner angle of mixed layer
R_{ML}		average density ratio of the mixed layer

comparison between the detected ~~gradient layer~~ interface characteristics of thermohaline staircases in three prevailing staircase regions and previous observations, suggested that the detection algorithm accurately captures ~~each~~ both double-diffusive ~~regime. Although the gradient layer height was slightly overestimated in two regions, the magnitude of the temperature and~~ regimes. The algorithm detected correct magnitudes of the conservative temperature and absolute salinity steps in the ~~gradient layers was correct~~interfaces, which allows for adequate estimates of the effective diffusivity in thermohaline staircases.

The global dataset resulting from the detection algorithm contains properties and characteristics of both mixed layers and ~~gradient layers~~interfaces. Combined with their locations, this data allows for a statistical analysis of thermohaline staircases on global ~~or regional~~ scales. For example, the global occurrence of thermohaline staircases could give insight in the contribution of double diffusion to the global mechanical energy budget. Moreover, the ~~gradient layer~~ interface characteristics can be used to validate model and laboratory results on how ~~double diffusive~~ double-diffusive mixing impacts the regional ocean circulation.

7 Code and data availability

Both algorithm and global dataset are available at doi: https://doi.org/10.5281/zenodo.4286170 (van der Boog et al., 2020a). The algorithm is written in Python3 and is available under the Creative Commons Attribution 4.0 License. More details on the functions and output of the algorithm are depicted in Table A1 and Table A2, respectively. The structure of the algorithm is displayed in Figure A4.

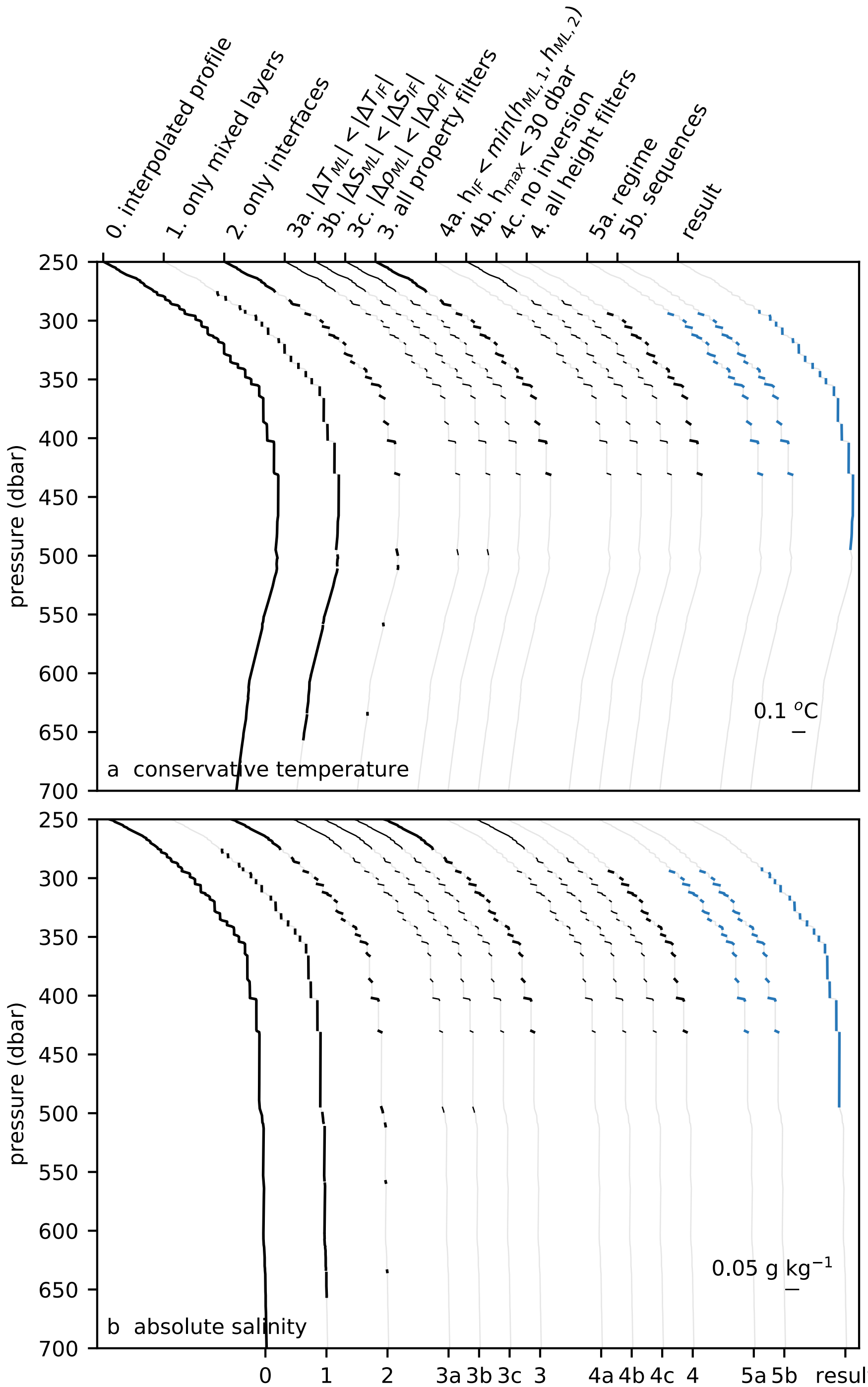

Figure A1. Steps of the detection algorithm applied on a profile in the Arctic Ocean, where steps are indicated on separate (a) conservative temperature and (b) absolute salinity profiles. Each profile is shifted for clarity. Similar to Figures 4-6, an interface is not considered by the detection algorithm when the interface characteristics did not meet the requirements of a previous step. Original profile is taken from Ice-Tethered-Profiler ITP64 at 137.8^{o}W and 75.2^{o}N on 29 January 2013. The details of the data preparation and the algorithm steps are discussed in Section 2 and Section 3, respectively.

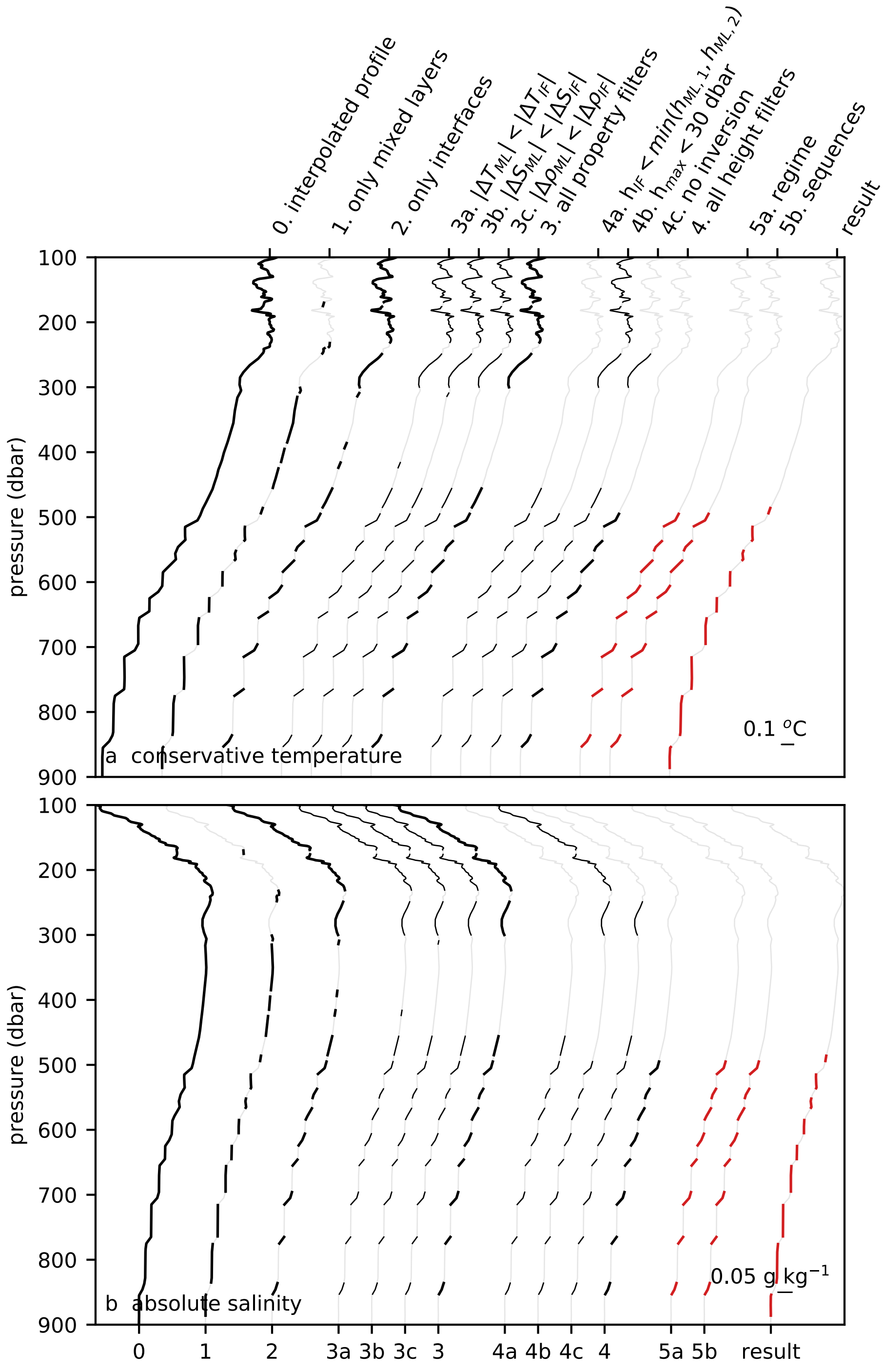

Figure A2. as Figure A1, but for a profile in the Mediterranean Sea. Original profile is taken from Argo float 6901769 at 8.9^{o}E and 37.9^{o}N on 31 October 2017.

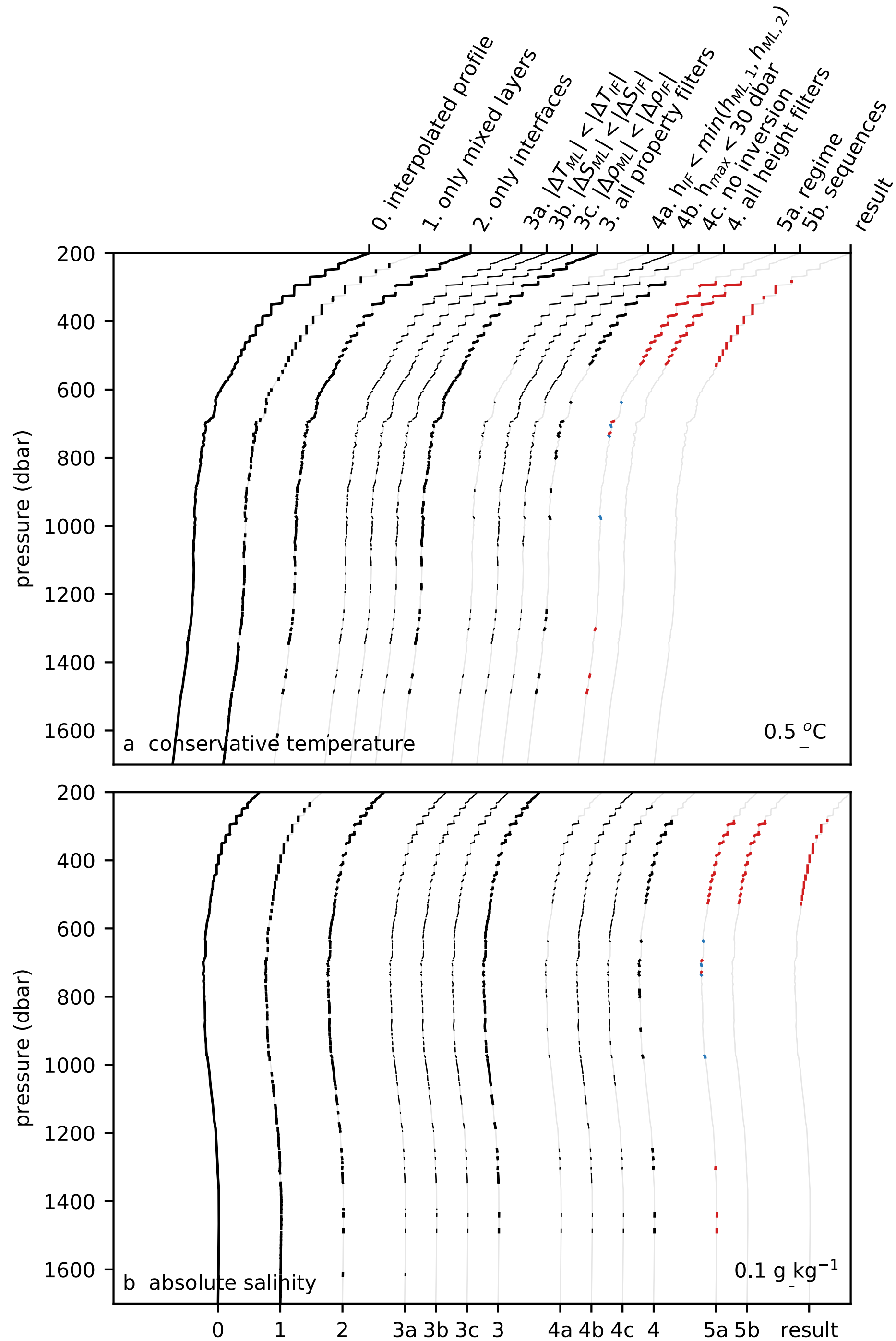

Figure A3. as Figure A1, but for a profile in the western tropical North Atlantic. Original profile is taken from Argo float 4901478 at 53.3°W and 11.6°N on 9 August 2014.

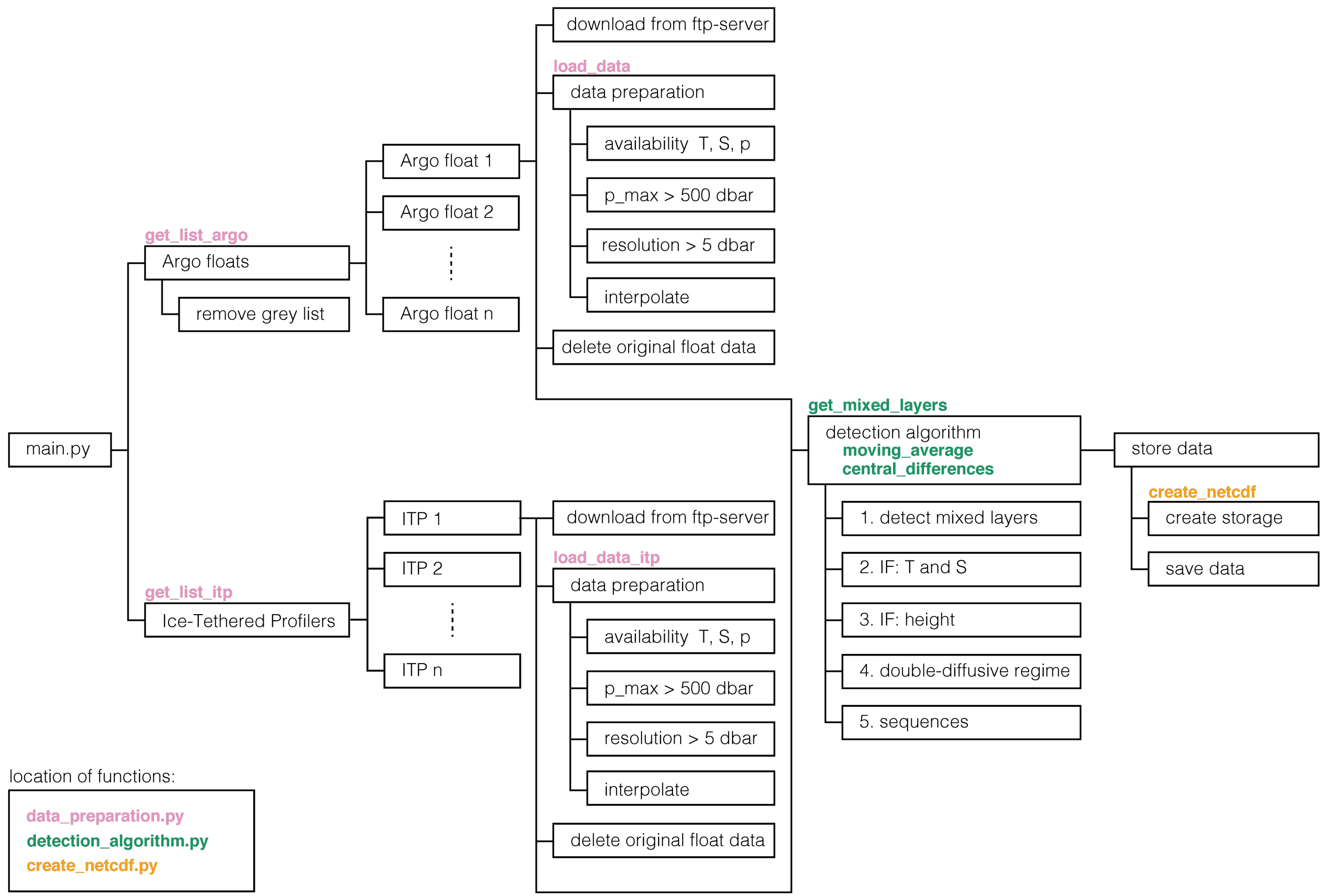

Figure A4. Structure of the software. Each step in the software is shown by a box. Whenever a particular step is contained inside a function, the name of the function is mentioned above the step. Details of the preprocessing of the data and the detection algorithm are discussed in Sections 2 and Section 3, respectively.

Author contributions. CvdB and OK designed the detection scheme. CvdB wrote the paper and was supervised CK, JP and HD who helped shape the analysis and paper.

Competing interests. The authors declare that they have no conflict of interest.

Acknowledgements. The Ice-Tethered Profiler data were collected and made available by the Ice-Tethered Profiler Program (Krishfield et al., 2008; Toole et al., 2011) based at Woods Hole Oceanogaphic Institution (http://www.whoi.edu/itp). The Argo data were collected and made freely available by the International Argo Program and the national programs that contribute to it (http://www.argo.ucsd.edu, http://argo.jcommops.org). The Argo Program is part of the Global Ocean Observing System (Argo, 2020). The work of Carine van der Boog is financed by a Delft Technology Fellowship awarded to Caroline Katsman.

References

Argo: Argo User's Manual V3.3, Ifremer, https://doi.org/10.13155/29825, 2019.

Argo: Argo Float Data and Metadata from Global Data Assembly Centre (Argo GDAC), https://doi.org/10.17882/42182, 2020.

Bebieva, Y. and Speer, K.: The Regulation of Sea Ice Thickness by Double-Diffusive Processes in the Ross Gyre, Journal of Geophysical Research: Oceans, 124, 7068–7081, https://doi.org/10.1029/2019JC015247, 2019.

Bebieva, Y. and Timmermans, M.-L.: The Relationship between Double-Diffusive Intrusions and Staircases in the Arctic Ocean, Journal of Physical Oceanography, 47, 867–878, https://doi.org/10.1175/JPO-D-16-0265.1, 2017.

Bryden, H. L., Schroeder, K., Sparnocchia, S., Borghini, M., and Vetrano, A.: Thermohaline Staircases in the Western Mediterranean Sea, Journal of Marine Research, 72, 1–18, https://doi.org/10.1357/002224014812655198, 2014.

Buffett, G. G., Krahmann, G., Klaeschen, D., Schroeder, K., Sallarès, V., Papenberg, C., Ranero, C. R., and Zitellini, N.: Seismic Oceanography in the Tyrrhenian Sea: Thermohaline Staircases, Eddies, and Internal Waves, Journal of Geophysical Research: Oceans, 122, 8503–8523, https://doi.org/10.1002/2017JC012726, 2017.

Dong, S., Sprintall, J., Gille, S. T., and Talley, L.: Southern Ocean Mixed-Layer Depth from Argo Float Profiles, Journal of Geophysical Research, 113, C06 013, https://doi.org/10.1029/2006JC004051, 2008.

Durante, S., Schroeder, K., Mazzei, L., Pierini, S., Borghini, M., and Sparnocchia, S.: Permanent Thermohaline Staircases in the Tyrrhenian Sea, Geophysical Research Letters, 46, 1562–1570, https://doi.org/10.1029/2018GL081747, 2019.

Fer, I., Nandi, P., Holbrook, W. S., Schmitt, R. W., and Páramo, P.: Seismic Imaging of a Thermohaline Staircase in the Western Tropical North Atlantic, Ocean Science, 6, 621–631, https://doi.org/10.5194/os-6-621-2010, 2010.

Fine, R. A.: Circulation of Antarctic Intermediate Water in the South Indian Ocean, Deep Sea Research Part I: Oceanographic Research Papers, 40, 2021–2042, https://doi.org/10.1016/0967-0637(93)90043-3, 1993.

Garaud, P.: Double-Diffusive Convection at Low Prandtl Number, Annual Review of Fluid Mechanics, 50, 275–298, https://doi.org/10.1146/annurev-fluid-122316-045234, 2018.

Gargett, A. E. and Holloway, G.: Sensitivity of the GFDL Ocean Model to Different Diffusivities for Heat and Salt, Journal of Physical Oceanography, 22, 1158–1177, https://doi.org/10.1175/1520-0485(1992)022<1158:SOTGOM>2.0.CO;2, 1992.

Graham, F. S. and McDougall, T. J.: Quantifying the Nonconservative Production of Conservative Temperature, Potential Temperature, and Entropy, Journal of Physical Oceanography, 43, 838–862, https://doi.org/10.1175/JPO-D-11-0188.1, 2013.

Holte, J., Talley, L. D., Gilson, J., and Roemmich, D.: An Argo Mixed Layer Climatology and Database, Geophysical Research Letters, 44, 5618–5626, https://doi.org/10.1002/2017GL073426, 2017.

Kelley, D. E.: Fluxes through Diffusive Staircases: A New Formulation, Journal of Geophysical Research, 95, 3365, https://doi.org/10.1029/JC095iC03p03365, 1990.

Krishfield, R., Toole, J., Proshutinsky, A., and Timmermans, M.-L.: Automated Ice-Tethered Profilers for Seawater Observations under Pack Ice in All Seasons, Journal of Atmospheric and Oceanic Technology, 25, 2091–2105, https://doi.org/10.1175/2008JTECHO587.1, 2008.

McDougall, T. J. and Barker, P. M.: Getting Started with TEOS-10 and the Gibbs Seawater (GSW) Oceanographic Toolbox, SCOR/IAPSO WG, 127, 1–28, 2011.

Merryfield, W. J.: Origin of Thermohaline Staircases, Journal of Physical Oceanography, 30, 1046–1068, https://doi.org/10.1175/1520-0485(2000)030<1046:OOTS>2.0.CO;2, 2000.

Merryfield, W. J., Holloway, G., and Gargett, A. E.: A Global Ocean Model with Double-Diffusive Mixing, Journal of Physical Oceanography, 29, 1124–1142, https://doi.org/10.1175/1520-0485(1999)029<1124:AGOMWD>2.0.CO;2, 1999.

Oschlies, A., Dietze, H., and Kähler, P.: Salt-Finger Driven Enhancement of Upper Ocean Nutrient Supply, Geophysical Research Letters, 30, n/a–n/a, https://doi.org/10.1029/2003GL018552, 2003.

Padman, L. and Dillon, T. M.: Vertical Heat Fluxes through the Beaufort Sea Thermohaline Staircase, Journal of Geophysical Research, 92, 10 799, https://doi.org/10.1029/JC092iC10p10799, 1987.

Polyakov, I. V., Pnyushkov, A. V., Rember, R., Ivanov, V. V., Lenn, Y.-D., Padman, L., and Carmack, E. C.: Mooring-Based Observations of Double-Diffusive Staircases over the Laptev Sea Slope*, Journal of Physical Oceanography, 42, 95–109, https://doi.org/10.1175/2011JPO4606.1, 2012.

Radko, T.: A Mechanism for Layer Formation in a Double-Diffusive Fluid, Journal of Fluid Mechanics, 497, 365–380, https://doi.org/10.1017/S0022112003006785, 2003.

Radko, T.: Double-Diffusive Convection, Cambridge University Press, Cambridge, https://doi.org/10.1017/CBO9781139034173, 2013.

Radko, T. and Smith, D. P.: Equilibrium Transport in Double-Diffusive Convection, Journal of Fluid Mechanics, 692, 5–27, https://doi.org/10.1017/jfm.2011.343, 2012.

Ruddick, B.: A Practical Indicator of the Stability of the Water Column to Double-Diffusive Activity, Deep Sea Research Part A. Oceanographic Research Papers, 30, 1105–1107, https://doi.org/10.1016/0198-0149(83)90063-8, 1983.

Ruddick, B. and Kerr, O.: Oceanic Thermohaline Intrusions: Theory, Double-Diffusion in Oceanography, 56, 483–497, https://doi.org/10.1016/S0079-6611(03)00029-6, 2003.

Rudels, B.: Arctic Ocean Circulation, Processes and Water Masses: A Description of Observations and Ideas with Focus on the Period Prior to the International Polar Year 2007–2009, Progress in Oceanography, 132, 22–67, https://doi.org/10.1016/j.pocean.2013.11.006, 2015.

Schmitt, R., Perkins, H., Boyd, J., and Stalcup, M.: C-SALT: An Investigation of the Thermohaline Staircase in the Western Tropical North Atlantic, Deep Sea Research Part A. Oceanographic Research Papers, 34, 1655–1665, https://doi.org/10.1016/0198-0149(87)90014-8, 1987.

Schmitt, R. W.: Form of the Temperature-Salinity Relationship in the Central Water: Evidence for Double-Diffusive Mixing, Journal of Physical Oceanography, 11, 1015–1026, https://doi.org/10.1175/1520-0485(1981)011<1015:FOTTSR>2.0.CO;2, 1981.

Schmitt, R. W.: Double Diffusion in Oceanography, Annual Review of Fluid Mechanics, 26, 255–285, https://doi.org/10.1146/annurev.fl.26.010194.001351, 1994.

Schmitt, R. W.: Enhanced Diapycnal Mixing by Salt Fingers in the Thermocline of the Tropical Atlantic, Science, 308, 685–688, https://doi.org/10.1126/science.1108678, 2005.

Schroeder, K., Chiggiato, J., Bryden, H. L., Borghini, M., and Ben Ismail, S.: Abrupt Climate Shift in the Western Mediterranean Sea, Scientific Reports, 6, 23 009, https://doi.org/10.1038/srep23009, 2016.

Shibley, N. C., Timmermans, M.-L., Carpenter, J. R., and Toole, J. M.: Spatial Variability of the Arctic Ocean's Double-Diffusive Staircase, Journal of Geophysical Research: Oceans, 122, 980–994, https://doi.org/10.1002/2016JC012419, 2017.

Stern, M. E.: The "Salt-Fountain" and Thermohaline Convection, Tellus, 12, 172–175, https://doi.org/10.3402/tellusa.v12i2.9378, 1960.

Stern, M. E.: Collective Instability of Salt Fingers, Journal of Fluid Mechanics, 35, 209–218, https://doi.org/10.1017/S0022112069001066, 1969.

Talley, L. D.: Antarctic Intermediate Water in the South Atlantic, pp. 219–238, Springer Berlin Heidelberg, Berlin, Heidelberg, https://doi.org/10.1007/978-3-642-80353-6_11, 1996.

Timmermans, M.-L., Garrett, C., and Carmack, E.: The Thermohaline Structure and Evolution of the Deep Waters in the Canada Basin, Arctic Ocean, Deep Sea Research Part I: Oceanographic Research Papers, 50, 1305–1321, https://doi.org/10.1016/S0967-0637(03)00125-0, 2003.

Timmermans, M.-L., Toole, J., Krishfield, R., and Winsor, P.: Ice-Tethered Profiler Observations of the Double-Diffusive Staircase in the Canada Basin Thermocline, Journal of Geophysical Research, 113, C00A02, https://doi.org/10.1029/2008JC004829, 2008.

Toole, J. M., Krishfield, R., Timmermans, M.-L., and Proshutinsky, A.: The Ice-Tethered Profiler: Argo of the Arctic, Oceanography, 24, 126–135, 2011.

Tsuchiya, M.: Circulation of the Antarctic Intermediate Water in the North Atlantic Ocean, Journal of Marine Research, 47, 747–755, https://doi.org/10.1357/002224089785076136, 1989.

van der Boog, C. G., Koetsier, J. O., Dijkstra, H. A., Pietrzak, J. D., and Katsman, C. A.: Data Supplement for 'Global Dataset of Thermohaline Staircases Obtained from Argo Floats and Ice-Tethered Profilers', https://doi.org/10.5281/ZENODO.4286170, 2020a.

van der Boog, C. G., Koetsier, J. O., Dijkstra, H. A., Pietrzak, J. D., and Katsman, C. A.: Global Dataset of Thermohaline Staircases, https://doi.org/10.4121/UUID:F6529D31-B285-46AC-990B-5F45839F4E11, 2020b.

Wong, A. P. S., Wijffels, S. E., Riser, S. C., Pouliquen, S., Hosoda, S., Roemmich, D., Gilson, J., Johnson, G. C., Martini, K., Murphy, D. J., Scanderbeg, M., Bhaskar, T. V. S. U., Buck, J. J. H., Merceur, F., Carval, T., Maze, G., Cabanes, C., André, X., Poffa, N., Yashayaev, I., Barker, P. M., Guinehut, S., Belbéoch, M., Ignaszewski, M., Baringer, M. O., Schmid, C., Lyman, J. M., McTaggart, K. E., Purkey, S. G., Zilberman, N., Alkire, M. B., Swift, D., Owens, W. B., Jayne, S. R., Hersh, C., Robbins, P., West-Mack, D., Bahr, F., Yoshida, S., Sutton, P. J. H., Cancouët, R., Coatanoan, C., Dobbler, D., Juan, A. G., Gourrion, J., Kolodziejczyk, N., Bernard, V., Bourlès, B., Claustre, H., D'Ortenzio, F., Le Reste, S., Le Traon, P.-Y., Rannou, J.-P., Saout-Grit, C., Speich, S., Thierry, V., Verbrugge, N., Angel-Benavides, I. M., Klein, B., Notarstefano, G., Poulain, P.-M., Vélez-Belchí, P., Suga, T., Ando, K., Iwasaska, N., Kobayashi, T., Masuda, S., Oka, E., Sato, K., Nakamura, T., Sato, K., Takatsuki, Y., Yoshida, T., Cowley, R., Lovell, J. L., Oke, P. R., van Wijk, E. M., Carse, F., Donnelly, M., Gould, W. J., Gowers, K., King, B. A., Loch, S. G., Mowat, M., Turton, J., Rama Rao, E. P., Ravichandran, M., Freeland, H. J., Gaboury, I., Gilbert, D., Greenan, B. J. W., Ouellet, M., Ross, T., Tran, A., Dong, M., Liu, Z., Xu, J., Kang, K., Jo, H., Kim, S.-D., and Park, H.-M.: Argo Data 1999–2019: Two Million Temperature-Salinity Profiles and Subsurface Velocity Observations From a Global Array of Profiling Floats, Frontiers in Marine Science, 7, 700, https://doi.org/10.3389/fmars.2020.00700, 2020.

Zodiatis, G. and Gasparini, G. P.: Thermohaline Staircase Formations in the Tyrrhenian Sea, Deep Sea Research Part I: Oceanographic Research Papers, 43, 655–678, https://doi.org/10.1016/0967-0637(96)00032-5, 1996.

Table A2. Functions used in the software.

function	input	output	description
get_list_argo	centers, filename	directory, floats, float_list	Access ftp server (ftp.ifremer.fr) and navigate through directories of the Data Assembly Centers (*centers*) to locate the Argo floats from the input list (*filename*). Directory of floats on the ftp-server are given in *directory*. The full list of Argo float before removal of the floats of the Grey list is given in *floats*. Argo floats mentioned on the Grey list are removed. Required packages: ftplib, numpy, pandas
get_list_itp	-	list of floats	Access ftp server (ftp.whoi.edu) to obtain list of available Ice-Tethered Profilers. Required packages: ftplib, numpy
load_data	filename, interp	p, lat, lon, ct, sa, juld	The profiles of a single Argo float (*filename*) are evaluated and linearly interpolated to a resolution of 1 dbar (*interp=True*). Only profiles with an average resolution is finer than 5 dbar and pressure levels exceeding 500 dbar are considered. Output contains interpolated data of pressure, latitude (*lat*), longitude (*lat*), conservative temperature (*ct*), absolute salinity (*sa*), Julian date (*juld*). Required packages: gsw, numpy, netCDF4, scipy
load_data_itp	path,profiles,interp	prof_no, p, lat, lon, ct, sa, juld	Similar as load_data, but then for Ice-Tethered Profilers. There is an additional output containing the FloatID of the ITP (*prof_no*). Required packages: datetime, gsw, numpy, pandas, scipy
get_mixed_layers	p, ct, sa, c1, c2, c3, c4	ml, gl, masks	This is the detection algorithm. Input contains the pressure, conservative temperature, absolute salinity and the user-defined input parameters: $\partial\sigma_1/\partial p_{max}$(*c1*), $\Delta\sigma_{1,ML,max}$ (*c2*), moving average window (*c4*), $h_{IF,max}$ (*c3*). The output are classes with the mixed layer characteristics (*ml*), interface characteristics (*gl*) and the masks (see Details in Table A1). Required packages: gsw, numpy, scipy.
moving_average2d	dataset, window	mav	